



The equilibrium response to idealized thermal forcings in a comprehensive GCM: implications for recent tropical expansion

R. J. Allen^{1,2,3}, S. C. Sherwood⁴, J. R. Norris², and C. S. Zender³

¹Department of Earth Sciences, University of California, Riverside, Riverside, CA, USA

²Scripps Institution of Oceanography, University of California, San Diego, CA, USA

³Department of Earth System Science, University of California, Irvine, CA, USA

⁴Climate Change Research Centre and ARC Centre of Excellence, University of New South Wales, Sydney, Australia

Correspondence to: R. J. Allen (rjallen@ucr.edu)

Received: 17 August 2011 – Published in Atmos. Chem. Phys. Discuss.: 2 December 2011

Revised: 22 March 2012 – Accepted: 11 May 2012 – Published: 31 May 2012

Abstract. Several recent studies have shown the width of the tropical belt has increased over the last several decades. The mechanisms driving tropical expansion are not well known and the recent expansion is underpredicted by state-of-the-art GCMs. We use the CAM3 GCM to investigate how tropical width responds to idealized atmospheric heat sources, focusing on zonal displacement of the tropospheric jets. The heat sources include global and zonally restricted lower-tropospheric warmings and stratospheric coolings, which coarsely represent possible impacts of ozone or aerosol changes. Similar to prior studies with simplified GCMs, we find that stratospheric cooling – particularly at high-latitudes – shifts jets poleward and excites Northern and Southern Annular Mode (NAM/SAM)-type responses. We also find, however, that modest heating of the midlatitude boundary layer drives a similar response; heating at high latitudes provokes a weaker, equatorward shift and tropical heating produces no shift. Over 70 % of the variance in annual mean jet displacements across 27 experiments is accounted for by a newly proposed “Expansion Index”, which compares mid-latitude tropospheric warming to that at other latitudes. We find that previously proposed factors, including tropopause height and tropospheric stability, do not fully explain the results. Results suggest recently observed tropical expansion could have been driven not only by stratospheric cooling, but also by mid-latitude heating sources due for example to ozone or aerosol changes.

1 Introduction

Recent observational analyses show the tropics have widened over the last several decades. Estimates range from 2–5° latitude since 1979 (Seidel et al., 2008) and are based on several metrics, including a poleward shift of the Hadley cell (Hu and Fu, 2007), increased frequency of high tropopause days in the subtropics (Seidel and Randel, 2007) and increased width of the region with tropical column ozone levels (Hudson et al., 2006). Studies have also inferred a poleward shift in the tropospheric jets, based on enhanced warming in the mid-latitude troposphere (Fu et al., 2006) and cooling in the mid-latitude stratosphere (Fu and Lin, 2011). Zhou et al. (2011) showed a poleward shift of cloud boundaries associated with the Hadley cell, as well as a poleward shift of the subtropical dry zones. Clearly, tropical expansion has important implications for both global, and regional climate.

Climate models also show current, and future, global warming is associated with tropical expansion. Using the Intergovernmental Panel on Climate Change (IPCC) Coupled Model Intercomparison Project, Phase 3 (CMIP3) simulations, Yin (2005) found a poleward shift in the mid-latitude storm tracks, which was accompanied by poleward shifts in surface wind stress and precipitation. Similarly, Lorenz and DeWeaver (2007) found a poleward shift (and strengthening) of the tropospheric jets in response to global warming, which was accompanied by poleward and upward shifts in transient kinetic energy and momentum flux. Lu et al. (2007) showed CMIP3 models yield poleward displacement (and weakening) of the Hadley cell and subtropical dry zones, which

is associated with an increase in extratropical tropopause height, and subtropical static stability. Models also show that tropical expansion projects onto the leading pattern of variability (Kushner et al., 2001), with about half of CMIP3 model-simulated Hadley cell and subtropical dry zone expansion during the next century explained by positive trends in the Northern and Southern Annular Mode (NAM/SAM) (Previdi and Liepert, 2007).

Although both GCMs and observations show tropical widening over the last 2–3 decades, models underestimate the magnitude of observed trends. For example, Johanson and Fu (2009) show the largest CMIP3 tropical widening trends are $\sim 1/5$ of the observed widening. This significant underestimation exists across five scenarios, as well as three separate definitions of Hadley cell width, including dynamical and hydrological definitions. Lu et al. (2009) used the GFDL atmospheric model AM2.1 to show observed changes in sea surface temperatures (SSTs) and sea-ice cannot explain increased tropical width, as defined by the tropopause probability density function. A similar simulation, however, that also included the direct radiative effects of anthropogenic and natural sources better reproduced the observed widening. Polvani et al. (2011) showed that broadening of the Hadley cell and poleward expansion of the subtropical dry zone over the latter half of the 20th century in the SH—particularly during December–January–February—have been primarily caused by polar stratospheric ozone depletion.

Idealized climate models (e.g., no moist processes, no topography) have been used to better understand the mechanisms involved with tropical expansion. Polvani and Kushner (2002) and Kushner and Polvani (2004) found that cooling of the polar winter stratosphere, which is associated with reduced stratospheric wave drag, results in a poleward tropospheric jet shift and strengthening of surface wind. Haigh et al. (2005) showed that uniform heating of the stratosphere (e.g., via increased solar or volcanic activity), or heating restricted to high-latitudes, forces the jets equatorward; heating in low latitudes forces them poleward.

Frierson et al. (2007) used both simple and comprehensive GCMs to show tropical expansion occurs with increased global mean temperature, and secondly, with an increased pole-to-equator temperature gradient. They argued that the response was due to increased static stability, which reduces baroclinic growth rates and pushes the latitude of baroclinic instability onset poleward, in agreement with the Hadley cell width scaling of Held (2000). This was further supported by Lu et al. (2008), who showed that poleward expansion of the Hadley cell and shift of the eddy-driven jet in CMIP3 global warming experiments are related to a reduction in baroclinicity, which is primarily caused by an increase in subtropical static stability. This relationship was most significant during austral summer (December–January–February), particularly in the Southern Hemisphere (SH).

Lorenz and DeWeaver (2007) showed that increasing the tropopause height (as expected in a warmer troposphere) in a simple dry GCM resulted in poleward jet displacement. This response was largest when the tropopause on the poleward flank of the jet was raised; however, the opposite response occurred if the tropopause was raised on the equatorward side of the jet. This tropopause–jet relationship is consistent with Williams (2006).

Recently, Butler et al. (2010) used a simplified GCM to try to attribute storm track shifts to temperature changes in particular regions. They found that warming in the tropical troposphere, or cooling in the high-latitude stratosphere, each shifted the storm tracks poleward, whereas polar surface warming shifted them equatorward. Such results are qualitatively consistent with earlier studies (Chen and Held, 2007; Chen et al., 2008), arguing that the observed poleward shift in the surface westerlies has been due to increased Rossby wave phase speeds, which results in poleward displacement of the region of wave breaking in the subtropics. Kidston et al. (2011) argued that an increase in eddy length scale, a robust response to global warming (Kidston et al., 2010), causes the poleward shift of the mid-latitude eddy-driven jet streams. Both Brayshaw et al. (2008) and Chen et al. (2010) used aquaplanet GCM simulations to show that high-latitude SST warming poleward of the climatological jet results in an equatorward jet displacement. For low-latitude warming that extends poleward of the climatological jet latitude, a poleward jet displacement occurred.

Expanding upon these studies, we use a comprehensive GCM to gain a better understanding of how tropical width—particularly tropospheric (850–300 hPa) jet displacement—responds to different types of simple heating at realistic amplitudes. The thermal forcings examined include zonally uniform heat sources in the troposphere or heat sinks in the stratosphere. Our study differs from past studies in specifying heat sources that are representative of possible non-CO₂ climatic forcings, rather than imposing characteristic temperature perturbations. Investigation of the effects of such heat sources on tropical width is of interest due to the significant 20th century increases in anthropogenic aerosols, including absorbing aerosols like black carbon (Bond et al., 2007) and reflecting aerosols like sulfate (Smith et al., 2011), as well as tropospheric ozone (Shindell et al., 2006) and ozone precursors (van Aardenne et al., 2001). Our objective is to clarify the sensitivity of tropical width to different types of heating, with the ultimate goals of gaining insight into the observed widening and better understanding of the responses seen in past GCM studies. Our results show the importance of perturbed tropospheric temperature gradients and a wave-modulated stratospheric pathway in driving zonal jet displacements. We also show that previously proposed tropical expansion mechanisms are unable to fully explain our results. We build upon these results in a subsequent paper, which will examine the responses to more realistic representations of non-CO₂ forcings. This paper is organized as follows: in

Sect. 2 we discuss the CAM GCM and our experimental design. In Sect. 3 we present the response to idealized stratospheric cooling and tropospheric heating, and compare these responses to a doubling of CO₂. Section 4 discusses expansion scenarios, including the tropospheric and stratospheric pathways. Conclusions are presented in Sect. 5.

2 Methods

2.1 CAM description

The Community Atmosphere Model (CAM) version 3 (Collins et al., 2004), is the fifth generation of the National Center for Atmosphere Research (NCAR) atmospheric General Circulation Model (GCM) and is the atmospheric component of the Community Climate System Model (CCSM). CAM uses a Eulerian spectral transform dynamical core, where variables are represented in terms of coefficients of a truncated series of spherical harmonic functions. The model time step is 20-min, and time integration is performed with a semi-implicit leapfrog scheme. The vertical coordinate is a hybrid coordinate, with 26 vertical levels. The model has a relatively poorly-resolved stratosphere, with ~ 9 levels above 100 hPa and a top level at 2.9 hPa. The total parameterization package consists of four basic components: moist precipitation processes/convection, clouds and radiation, surface processes, and turbulent mixing. The land surface model is the Community Land Model (CLM) version 3 (Oleson et al., 2004), which combines realistic radiative, ecological and hydrologic processes.

2.2 Experimental design

CAM is run at T42 resolution ($\sim 2.8 \times 2.8^\circ$) with a slab ocean-thermodynamic sea ice model. All experiments are run for at least 70 yr, the last 30 of which are used in this analysis, during which the model has reached equilibrium (i.e., no significant trend in TOA net energy flux).

Stratospheric cooling experiments (10PLO3; see Table 1) were performed by reducing the stratospheric ozone by 10 % globally, as well as individually for the tropics ($\pm 30^\circ$), mid-latitudes (30–60° N/S) and high-latitudes (60–90° N/S). The stratosphere is defined as the model levels above the tropopause, which is estimated by a thermal definition using the method of Reichler et al. (2003). We use CAM's default ozone boundary data set, which contains zonal monthly ozone volume mixing ratios, and reduce the ozone by 10 % at the appropriate latitudes and stratospheric pressures on a monthly basis. A 10 % ozone reduction is in rough agreement with the change in stratospheric ozone from 1979–2000 (Newchurch et al., 2003). The ozone perturbation is seasonally invariant, as are all perturbations in this study, and is not meant to represent the real seasonal cycle of ozone change.

Our standard set of tropospheric heating experiments (LTHT) adds a 0.1 K day^{-1} ($\sim 3.5 \text{ W m}^{-2}$) heating source to

the lower troposphere (surface to ~ 700 hPa). Such a heating rate is comparable to recent satellite-based estimates of present-day anthropogenic aerosol solar absorption (Chung et al., 2005). We conduct a globally uniform heating experiment, as well as latitudinally restricted heating of the tropics, mid- and high-latitudes. Although heating is only applied to the lower troposphere, the globally uniform temperature response resembles that based on a doubling of CO₂. This is due to destabilization of the lower atmosphere and increased convection, which vertically redistributes the heat throughout the depth of the troposphere. Similar experiments with mid-tropospheric and upper-tropospheric heating do not destabilize the lower atmosphere, and result in maximum tropospheric warming near the altitude of heat input. Table 2 lists the suite of tropospheric heating experiments. In all cases, the response is estimated as the difference between the experiment and a corresponding control, which lacks the added heat source.

A standard global warming experiment is also performed, where the CO₂ volume mixing ratio is doubled from 3.55×10^{-4} to 7.10×10^{-4} . We also conduct an extreme global warming experiment, where the CO₂ volume mixing ratio is increased by a factor of eight. The resulting climate signals are named $2 \times \text{CO}_2$ and $8 \times \text{CO}_2$, respectively.

We compare our CAM integrations to 12 $2 \times \text{CO}_2$ CMIP3 equilibrium (slab ocean) experiments, as well as 10 1 % to $4 \times \text{CO}_2$ transient CMIP3 experiments. Table 3 lists the CMIP3 models used in this study. For the 1 % to $4 \times \text{CO}_2$ experiments, we compare the 25 yr prior to CO₂ quadrupling (years 115–139) to the corresponding control.

Finally, we evaluate the robustness of some of our CAM results – specifically the response to lower tropospheric heating – using an alternate GCM, the GFDL AM2.1 (Anderson et al., 2004). Because the GFDL model does not include a slab ocean model, these experiments are run with climatological SSTs. GFDL experiments are integrated for 40 yr, the last 30 of which are used to estimate the climate response.

2.3 Measures of tropical width and its changes

2.3.1 Tropospheric jet

Several jet-based measures of tropical width were explored. This includes the latitude of the main jet, which we locate by finding the maximum of the zonally and monthly averaged zonal wind (U) in either hemisphere (NH or SH). The poleward jet displacements are then estimated by taking the difference of the mean jet location (experiment minus control) in either hemisphere. We computed this measure on each pressure level and averaged the 850–300 hPa displacements to obtain a tropospheric jet displacement. Because our jet definition is based on the entire troposphere, it primarily represents the subtropical jet, and secondarily the mid-latitude eddy-driven jet. Displacements of the tropospheric and eddy-driven jet, however, are closely related;

Table 1. Stratospheric cooling experiments.

Signal	Description
10PLO3	Global 10 % reduction in stratospheric ozone
10PLO3 _{TR}	As 10PLO3, but ozone reduced over tropics ($\pm 30^\circ$) only
10PLO3 _{ML}	As 10PLO3, but ozone reduced over mid-latitudes (30–60° N/S)
10PLO3 _{HL}	As 10PLO3, but ozone reduced over high-latitudes (60–90° N/S)

Table 2. Tropospheric heating experiments.

Signal	Description
LTHT	Global lower-tropospheric (surface to ~ 700 hPa) heating of 0.1 K day^{-1}
LTHT _{TR}	As LTHT, but heating of tropics ($\pm 30^\circ$) only
LTHT _{ML}	As LTHT, but heating of mid-latitudes (30–60° N/S)
LTHT _{HL}	As LTHT, but heating of high-latitudes (60–90° N/S)
LTHT _{TRML}	As LTHT, but heating of tropics and mid-latitudes ($\pm 60^\circ$)
LTHT _{MLHL}	As LTHT, but heating of mid- and high-latitudes (± 30 – 90°)
LTHT2x	As LTHT, but double the heating rate (0.2 K day^{-1})
LTHT4x	As LTHT, but quadruple the heating rate (0.4 K day^{-1})
MTHT	Heating the mid-troposphere (~ 700 – 400 hPa)
UTHT _{ML}	Mid-latitude heating of the upper troposphere (4 levels below tropopause)
LTHT _{10PLO3}	Global lower-tropospheric heating of 0.1 K day^{-1} and 10 % reduction in stratospheric ozone

Table 3. Definition of the CMIP3 $2\times\text{CO}_2$ equilibrium (slab ocean) and the 1 % to $4\times\text{CO}_2$ transient experiments used in this study. A “Y” (“N”) indicates this model was (was not) used for the given experiment.

Model Acronym	Institution	$2\times\text{CO}_2$	$4\times\text{CO}_2$
CCSM3	National Center for Atmospheric Research	Y	Y
CGCM3.1(T47)	Canadian Center for Climate Modeling and Analysis	Y	Y
CGCM3.1(T63)	Canadian Center for Climate Modeling and Analysis	Y	N
CSIRO-Mk3.0	CSIRO Atmospheric Research	Y	N
ECHAM5/MPI-OM	Max Plank Institute for Meteorology	Y	N
GFDL-CM2.0	Geophysical Fluid Dynamics Laboratory	Y	Y
GFDL-CM2.1	Geophysical Fluid Dynamics Laboratory	N	Y
GISS-ER	Goddard Institute for Space Studies	Y	Y
INM-CM3.0	Institute for Numerical Mathematics	Y	Y
IPSL-CM4	Institut Pierre Simon Laplace	N	Y
MIROC3.2(hires)	Center for Climate System Research/NIES ^a /JAMSTEC ^b	Y	N
MIROC3.2(medres)	Center for Climate System Research/NIES ^a /JAMSTEC ^b	Y	Y
MRI-CGCM2.3.2	Meteorological Research Institute	Y	Y
PCM	National Center for Atmospheric Research	N	Y
UKMO-HadGEM1	Hadley Center for Climate Prediction and Research	Y	N

^a NIES is the National Institute for Environmental Studies.

^b JAMSTEC is the Frontier Research Center for Global Change in Japan.

the correlation between $2\times\text{CO}_2$ CMIP3 jet displacements using the annual mean 850–300 hPa U maximum and the near-surface (10-m) U maximum – which others have used as a measure of the eddy-driven jet (e.g., Kidston and Gerber, 2010) – is 0.83 in the NH and 0.90 in the SH. The correlation is weakest during JJA in the SH ($r = 0.57$), which is consistent with a winter-time decoupling of the subtropical and

eddy jets, resulting in a double jet structure (e.g., Gallego et al., 2005).

We also investigated an additional method for locating the jet, where we located the “sides” of the jet and then found their midpoint; the sides were based on a specified percentile value of zonal wind. Although both methods yielded similar displacements, testing indicated that the percentile method yielded somewhat more stable results; thus only the results

from the percentile method, using the 75th percentile (p75), are shown. We do note, however, that the percentile method yields smaller displacements than the maximum method, and as the percentile is decreased (e.g., from 95 to 70), consistently smaller jet displacements are obtained. This is illustrated in Fig. 1, which compares tropospheric jet displacements in 12 CMIP3 2×CO₂ equilibrium experiments using the maximum method, and the percentile method (with p75). A correlation of 0.95 shows both methods yields similar displacements; however, displacements tend to be larger with the jet maximum approach. The ensemble annual mean jet displacement using the maximum method is 0.62° in the NH and 0.96° in the SH; corresponding values using p75 are 0.46° and 0.73°. This result shows the jet displacement is non-uniform.

Figure 1 also shows the CMIP3 4×CO₂ ensemble annual zonal mean tropospheric jet response, and the corresponding control. The response is not a uniform jet shift; there is some distortion of its shape, resulting in a poleward skew, which is larger for the faster winds. This is particularly evident in the SH, and helps to explain the larger poleward displacements with the jet maximum method. Similar, but weaker results exist for the 2×CO₂ equilibrium experiments (not shown).

2.3.2 Other measures

Additional measures of tropical displacement (Johanson and Fu, 2009) include (1) the latitude of the subtropical Mean Meridional Circulation (MMC) minima, defined as the latitudes where the MMC at 500 hPa becomes zero poleward of the subtropical maxima; and (2) the latitudes where precipitation minus evaporation ($P - E$) becomes zero on the poleward side of the subtropical minima (a measure of subtropical dry zone expansion). All displacements are estimated by first smoothing the zonal monthly mean of the appropriate model field(s) and interpolating to 0.5° resolution using cubic splines. Smoothing was performed by taking a running mean over ~10 degrees of latitude. Nearly identical results are obtained without interpolating.

In addition to zonal displacements, we also quantify the changes in the strength and altitude of the jet. The altitude of the jet was quantified by interpolating the zonal wind to 10 hPa vertical resolution, and locating the pressure of maximum monthly zonal wind. This procedure is only done poleward of ~20°, since the jet is not well defined in the tropics. The strength of the jet was quantified by locating the maximum zonal wind in each hemisphere for each pressure level and month. A similar procedure was used to quantify the strength of the Hadley circulation, using the maximum magnitude (i.e., absolute value) of the tropical MMC at 500 hPa. The change in strength or jet altitude is then estimated as the difference between experiment and control.

Throughout this manuscript, statistical significance is estimated with a standard t -test, using the pooled variance. The influence of serial correlation is accounted for by using the

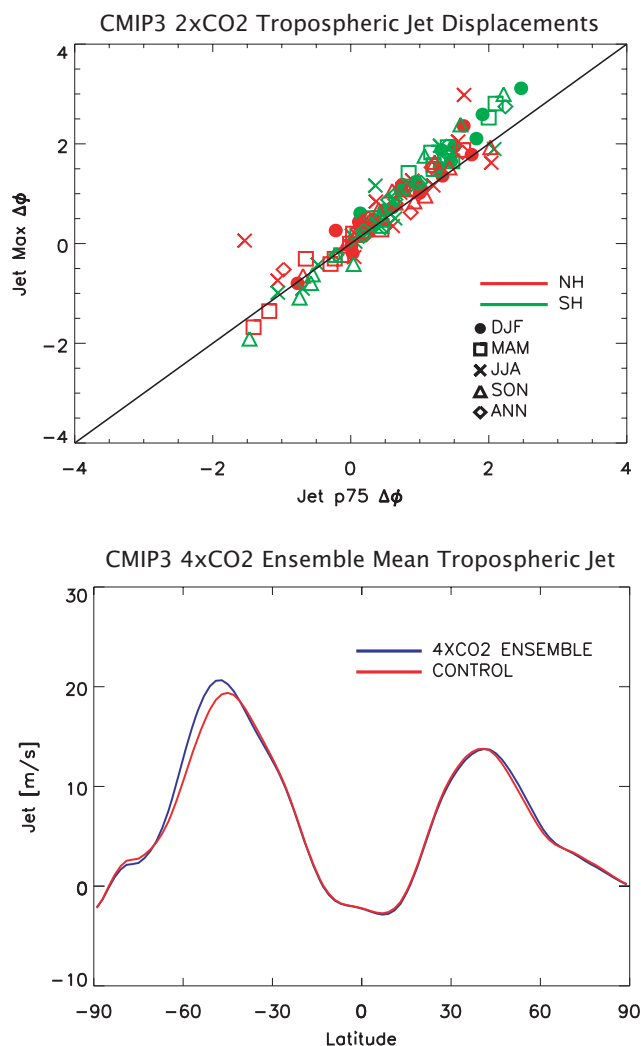


Fig. 1. (Top panel) Tropospheric poleward jet displacement [degrees latitude] based on 12 CMIP3 2×CO₂ equilibrium experiments using the maximum zonal wind method (Jet Max) and the percentile method with the 75th percentile (Jet p75). (Bottom panel) The ensemble annual zonal mean tropospheric jet (850–300 hPa U) response based on 10 1% to 4×CO₂ transient CMIP3 experiments, along with the corresponding control.

effective sample size, $n(1 - \rho_1)(1 + \rho_1)^{-1}$, where n is the number of years and ρ_1 is the lag-1 autocorrelation coefficient (Wilks, 1995).

3 Results

3.1 Response to stratospheric cooling

Figure 2 shows the annual and zonal mean temperature and wind response for the stratospheric cooling (10PLO3) experiments. Also included is the meridional temperature gradient (T_y) response, with Southern Hemisphere (SH) T_y multiplied by -1 (and in all subsequent figures) so that

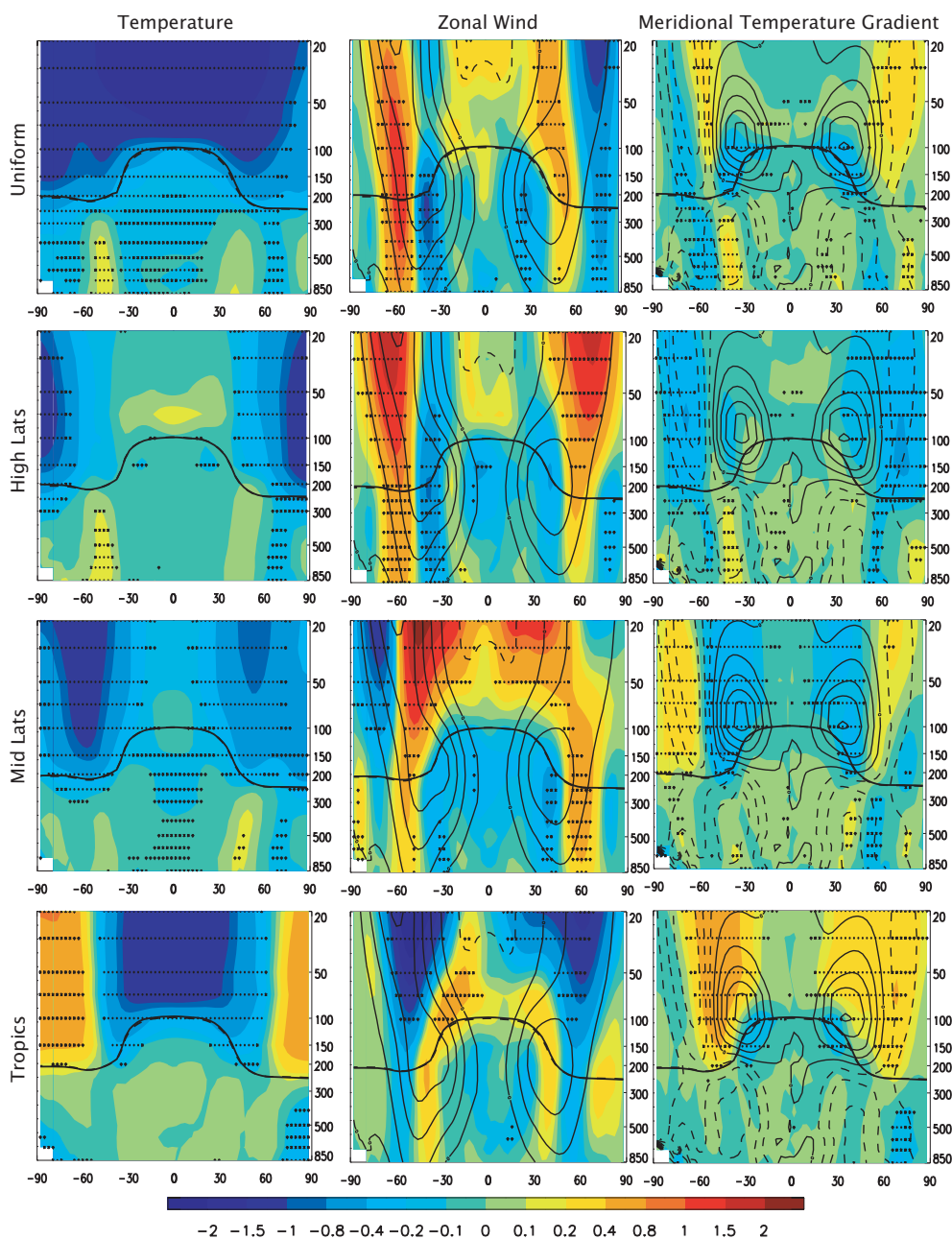


Fig. 2. Zonal annual mean (left) temperature, (center) zonal wind and (right) meridional temperature gradient response for 10PLO3 at (top) all latitudes, (middle top) high latitudes, (middle bottom) mid-latitudes and (bottom) low latitudes. Also shown is the tropopause pressure for the (dashed) control and (solid) experiment. Symbols represent significance at the 90 % (diamond); 95 % (cross) and 99 % (dot) confidence level. Climatological U (T_y) contour interval is 10 m s^{-1} ($2 \times 10^{-3} \text{ K km}^{-1}$) with negative values dashed. T units are K.

negative T_y always represents colder air poleward. As expected, temperatures are generally colder, by $\sim 1 \text{ K}$, because of reduced solar absorption where the ozone reduction was imposed. Several non-local responses also occur, including tropospheric warming for the all-, high-, and mid-latitude experiments. These three experiments also yield an increase in zonal wind (U) near 60° , whose magnitude decays downward through the troposphere. This U increase occurs near

the poleward flank of the tropospheric jet, while an opposite signed anomaly appears near the equatorward flank, indicating a poleward jet displacement. Note that reducing stratospheric ozone in the tropics (10PLO3_{TR}) yields the opposite response; however, the magnitude of the tropospheric wind anomaly is weak and not significant.

Table 4 quantifies the annual mean poleward displacement of the tropospheric (850–300 hPa) jets. As suggested by

Table 4. Tropospheric (850–300 hPa) poleward jet displacements for the (top) stratospheric cooling experiments and (middle and bottom) tropospheric heating/global warming experiments. Units are degrees latitude. CAM experiment significance is based on a Student's *t*-test and is denoted by bold ($\geq 90\%$); * ($\geq 95\%$) and ** ($\geq 99\%$). Also included is the corresponding jet displacement based on the ensemble mean of 12 CMIP3 $2\times\text{CO}_2$ equilibrium experiments and 10 CMIP3 $4\times\text{CO}_2$ transient experiments.

Signal	ANN		DJF		MAM		JJA		SON	
	NH	SH	NH	SH	NH	SH	NH	SH	NH	SH
10PLO3	0.30	0.59*	0.35	0.64	0.67	0.10	-0.15	0.72	0.38	0.87*
10PLO3 _{HL}	0.31	0.40*	-0.07	0.47	0.84	0.31	0.39	0.13	0.12	0.69*
10PLO3 _{ML}	0.40	0.26	0.42	0.05	0.60	0.19	0.34	0.04	0.31	0.81*
10PLO3 _{TR}	-0.04	-0.12	-0.20	-0.50	-0.01	-0.60	-0.05	0.32	0.14	0.30
LTHT	0.33	-0.13	0.49	-0.17	0.70	-0.34	-0.01	-0.17	0.17	0.18
LTHT _{HL}	-0.26	-0.16	-0.26	0.01	-0.14	-0.46	-0.65	-0.18	-0.06	0.01
LTHT _{ML}	0.66*	1.02**	0.34	0.89**	0.79	0.92**	0.74	1.15*	0.78**	1.16*
LTHT _{TR}	-0.05	-0.09	0.23	-0.63	0.28	-0.31	-0.49	0.42	-0.22	0.16
LTHT2x	0.12	-0.73**	0.66	-0.94**	0.67	-0.60	-0.64	-0.40	-0.21	-0.95*
LTHT2x _{HL}	-0.32	-0.42*	-0.19	-0.77*	0.19	-0.77*	-0.94	-0.11	-0.29	0.06
LTHT2x _{ML}	1.67**	0.85*	1.90**	0.72*	1.70**	1.01**	1.56**	0.93	1.56**	0.65
LTHT2x _{TR}	-0.20	-0.03	0.39	-0.32	0.36	-0.57*	-1.22**	0.54	-0.26	0.18
LTHT4x	-0.34	-1.12**	0.63*	-1.37**	-0.06	-1.03**	-1.49**	-1.05*	-0.41	-0.97**
LTHT4x _{TR}	-0.06	0.26	1.20**	0.27	1.32**	-0.93*	-1.8**	1.04*	-0.97**	0.72*
UTH _{ML}	0.65*	0.53**	0.59	0.22	1.10*	0.75*	0.43	0.53	0.46	0.69
$2\times\text{CO}_2$	1.08**	0.09	1.34**	-0.10	1.70**	0.28	0.50	0.35	0.71**	-0.20
$8\times\text{CO}_2$	1.50**	0.03	1.44**	-0.21	2.65**	1.27**	0.55	0.04	1.50**	-1.05*
$2\times\text{CO}_2$ CMIP3	0.46	0.73	0.58	1.22	-0.01	1.13	0.56	0.36	0.67	0.20
$4\times\text{CO}_2$ CMIP3	0.98	1.74	0.66	1.72	0.81	2.20	1.54	1.91	0.98	1.14

Fig. 2, stratospheric cooling generally yields a poleward displacement, of about 0.5° in each hemisphere. Cooling in the tropical stratosphere yields the opposite, but the equatorward shift is small and not significant. Note that these changes are generally similar in both hemispheres, and across the four seasons. Furthermore, Table 5 shows the additional metrics of tropical displacement are generally consistent with the jet response. For 10PLO3, 10PLO3_{HL} and 10PLO3_{ML}, both $P - E$ and MMC yield annual mean poleward displacement, although smaller than that based on the tropospheric jet.

3.2 Response to tropospheric heating

3.2.1 Sensitivity to the latitudinal distribution of near-surface heating

Figure 3 shows the T , U and T_y response for the lower tropospheric heating experiments (LTHT). Similar to CO_2 forcing, globally uniform near-surface heating causes a local warming maximum in the tropical upper troposphere due to moist convection, and high-latitude near-surface warming amplification due to snow and ice albedo feedbacks, as well as the higher static stability in polar regions. The zonal wind response to LTHT implies a poleward displacement of the NH tropospheric jet, but not the SH one. These shifts, however, are not statistically significant (see Table 4) in the annual mean or in any season. We note that in coupled ocean-

atmosphere models (and observations), the SH warming will be much less than that here due to uptake of heat by the Southern Ocean, which will affect how much the jet shifts.

Heating the individual latitude bands separately yields maximum warming at the heated latitudes, though with some spillover to most of the troposphere in the cases of LTHT_{HL} and LTHT_{ML}. Generally, however, the latitudes that are heated experience the largest temperature response, which is consistent with a down-gradient eddy heat flux response (i.e., oriented away from the latitude of maximum heating; not shown). There are also some dynamically induced remote cooling responses, including significant stratospheric cooling for LTHT and weaker tropospheric high-latitude cooling for LTHT_{TR}.

A much stronger impact on tropical width occurs with heating restricted to midlatitudes than for the globally uniform case. LTHT_{ML} shows both reduced U on the equatorward flank of the jet and increased U on the poleward jet flank, yielding significant poleward jet displacement of 0.66° in the NH and 1.02° in the SH. Significant displacements also occurred in experiments where either low or high latitudes were heated at the same time as mid-latitudes (LTHT_{TRML} and LTHT_{MLHL}, respectively), supporting the robustness of this result. For example, Table 5 shows simultaneous heating of the low- and mid-latitudes yields a poleward jet displacement of 0.41° in the NH and 0.20° in the SH. LTHT_{TRML} jet displacements become significant, and

Table 5. Annual mean poleward displacement (degrees latitude) of several measures of tropical width for the (top) stratospheric cooling experiments and (middle and bottom) tropospheric heating/global warming experiments, including the CMIP3 2×CO₂ and 4×CO₂ ensemble mean. These measures are based on the subtropical dry zone (precipitation minus evaporation, $P - E$), mean meridional mass circulation (MMC) and the tropospheric (850–300 hPa) jet. See text for further description. Significance is denoted as in Table 4.

Signal	P–E		MMC		Jet	
	NH	SH	NH	SH	NH	SH
10PLO3	0.29	0.30**	0.11	0.15	0.30	0.59*
10PLO3 _{HL}	0.21	0.22*	0.04	0.17	0.31	0.40*
10PLO3 _{ML}	0.23	0.23*	0.12	0.13	0.40	0.26
10PLO3 _{TR}	−0.13	0.03	−0.18	−0.02	−0.04	−0.12
LTHT	0.14	0.21*	−0.02	0.02	0.33	−0.13
LTHT _{HL}	−0.13	0.13	−0.07	0.03	−0.26	−0.16
LTHT _{ML}	0.61**	0.67**	0.32*	0.29**	0.66*	1.02**
LTHT _{TR}	−0.18	0.01	−0.17	−0.11	−0.05	−0.09
LTHT2x	0.16	0.01	−0.16	−0.04	0.12	− 0.73**
LTHT2x _{HL}	− 0.41**	0.02	−0.17	−0.13	−0.32	− 0.42*
LTHT2x _{ML}	1.03**	0.64**	0.79**	0.33*	1.67**	0.85*
LTHT2x _{TR}	− 0.34*	0.01	− 0.36**	−0.07	−0.20	−0.03
MTHT2x	0.66**	0.41**	0.47**	0.18	0.74*	0.48*
MTHT2x _{HL}	− 0.30*	− 0.22*	−0.10	−0.11	−0.29	− 0.69**
MTHT2x _{ML}	1.16**	1.03**	0.91**	0.40**	1.46**	1.29**
MTHT2x _{TR}	− 0.43**	0.05	−0.10	0.23*	0.02	0.45*
LTHT4x	−0.18	−0.05	− 0.31*	−0.14	−0.34	− 1.12**
LTHT4x _{TR}	− 0.41**	0.06	− 0.43**	0.11	−0.06	0.26
MTHT	0.24	0.20*	0.01	0.10	0.31	0.23
MTHT4x	0.74**	0.55**	0.41**	0.32**	0.74**	0.42*
UTHT _{ML}	0.40**	0.26*	0.28*	0.20*	0.65*	0.53**
LTHT _{TRML}	0.34*	0.29**	0.02	0.02	0.41	0.20
LTHT2x _{TRML}	0.60**	0.36**	0.21	0.18*	0.97**	0.53**
LTHT _{MLHL}	0.28*	0.33**	0.16	0.07	0.28	0.14
LTHT2x _{MLHL}	0.56**	0.56**	0.43**	0.33**	0.43	0.39
LTHT _{10PLO3}	0.02	0.11	−0.09	−0.02	−0.13	−0.32
LTHT2x _{10PLO3}	0.26*	0.25*	0.01	0.11	0.18	−0.01
LTHT4x _{10PLO3}	0.17	0.05	−0.07	−0.06	−0.20	− 0.92*
2×CO ₂	0.83**	0.60**	0.81**	0.42**	1.08**	0.09
8×CO ₂	0.85**	1.56**	1.48**	1.41**	1.50**	0.03
2×CO ₂ CMIP3	0.31	0.90	0.52	0.86	0.46	0.73
4×CO ₂ CMIP3	1.23	1.33	0.73	1.34	0.98	1.74

approximately double in magnitude, when the heating rate is doubled (LTHT2x_{TRML}).

Heating at high-latitudes (LTHT_{HL}) produced an opposite result, reducing U on the poleward jet flank to produce an equatorward jet displacement of -0.42° over the two hemispheres, about a quarter of the poleward shift with midlatitude heating. Tropical heating (LTHT_{TR}) increased the peak U throughout the atmosphere, but without significantly shifting the jet position except upward. While the above conclusions are based on jet shifts, similar responses are found among other tropical displacement measures (Ta-

ble 5), especially for the midlatitude heating which produced the strongest response.

Figure 4 shows the poleward displacement of the maximum meridional tropospheric temperature gradient, and the jet, for LTHT experiments as a function of pressure. LTHT_{HL} yields equatorward displacement of the maximum T_y whereas LTHT_{ML} features poleward displacement. This is consistent with the corresponding LTHT_{HL} and LTHT_{ML} tropospheric jet displacement – both quantities move poleward or equatorward together, in general agreement with thermal wind balance. For LTHT_{ML}, heating of the mid-latitudes

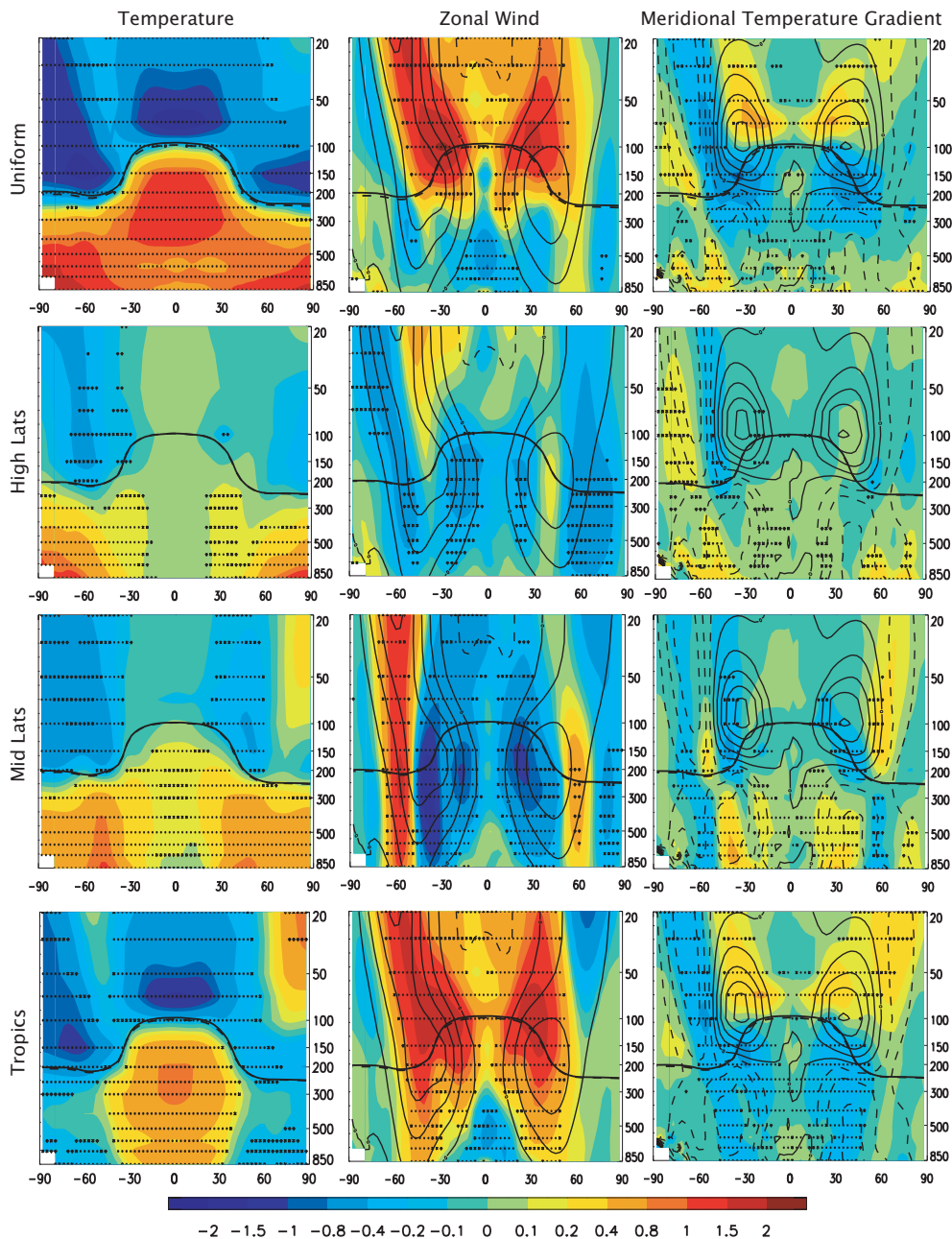


Fig. 3. As in Fig. 2, but based on the lower tropospheric heating (LTHT) experiments.

weakens the temperature gradient on the equatorward flank of the maximum T_y , but increases it on the poleward flank, as shown in Fig. 3. The tropospheric jet then responds by shifting poleward. The opposite occurs for LTHT_{HL} . Small displacements of the maximum T_y generally occur for LTHT_{TR} , in agreement with the small jet displacement. Over all experiments included in Fig. 4, the correlation between displacements of the maximum T_y and tropospheric jet is 0.81 in the NH and 0.92 in the SH. Although not shown, displacements of the maximum T_y are also similar to that of the tropospheric jet for the stratospheric cooling experiments.

Butler et al. (2010, 2011) also examined the impact of tropical heating, and found a shift similar to that obtained here with heating from $0\text{--}60^\circ$ N/S ($\text{LTHT}_{\text{TRML}}$), in contrast to our null result with tropical-only heating. While this result seems contradictory, the tropical heating employed by Butler et al. (2010, 2011) differed from ours by projecting significantly onto the mid-latitude isentropes, weakening baroclinicity in the subtropics while strengthening it in the mid-latitudes. Poleward jet displacement is also absent in $\text{LTHT}_{4\times\text{TR}}$ (Table 4), which features a heating rate more comparable to Butler et al. (2010, 2011). These results taken

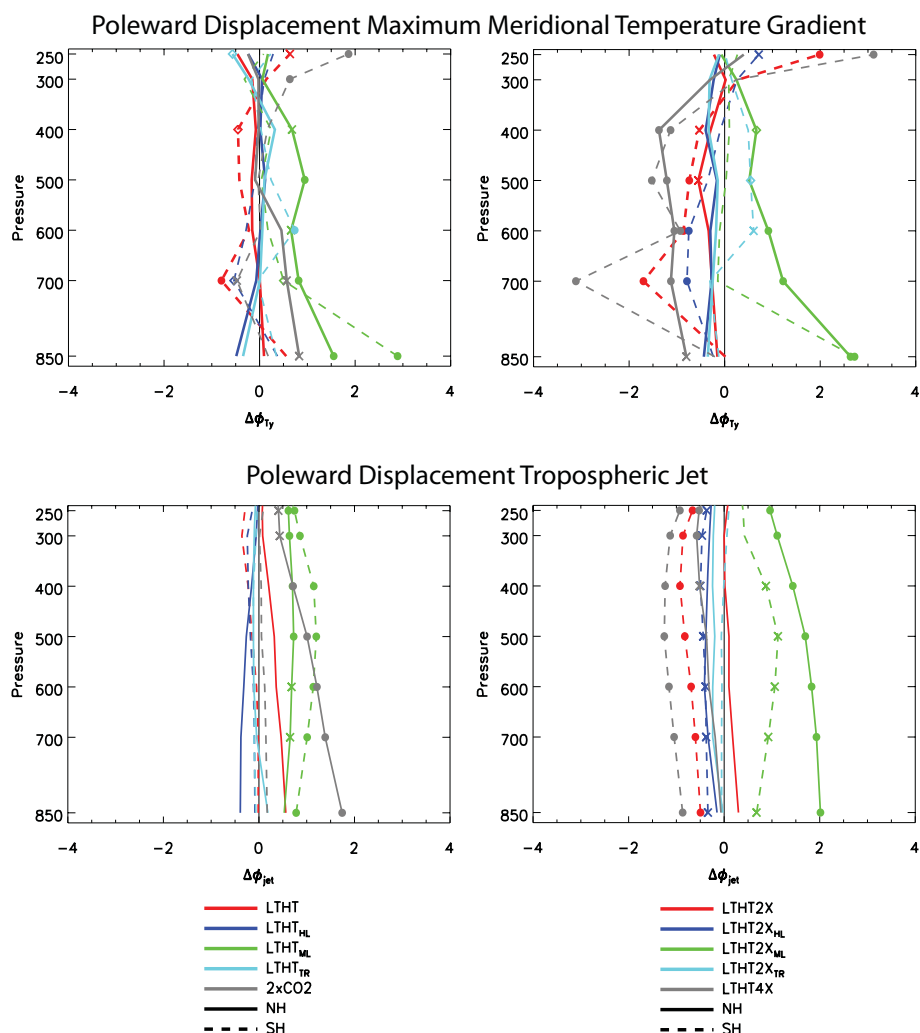


Fig. 4. Poleward displacement of the (top) latitude of the maximum tropospheric temperature gradient (T_y) and (bottom) jet for the Northern (solid) and Southern (dashed) Hemisphere for various LTHT and $2\times\text{CO}_2$ experiments. Symbols represent significance at the 90 % (diamond); 95 % (cross) and 99 % (dot) confidence level.

together are consistent with a particular sensitivity of the jet to heating in highly baroclinic, midlatitude regions, with relatively little sensitivity in the tropics.

Figure 5 further shows that geostrophic adjustment to the altered meridional temperature gradient explains most of the annual mean tropospheric wind response. Zonal wind shear for each pressure level is estimated from the corresponding meridional temperature gradient, according to thermal wind balance. To estimate the zonal wind, we use the 900 hPa zonal wind as a boundary condition. Taking the difference between the experiment and control yields the corresponding response, as shown in the center panel of Fig. 5. The actual zonal wind response closely corresponds to that estimated from thermal wind balance. The difference between the two (estimate – actual) shows no significant differences at most latitudes, except near the equator where meridional temperature gradients are small and geostrophy becomes a

poor approximation. Thus, most of the tropospheric jet shift in our LTHT experiments is consistent with a geostrophic adjustment to the altered meridional temperature gradient.

Although the eddy-driven jet is not the focus of this study, in our experiments displacements of the surface wind (a measure of the eddy-driven jet) are similar to those of the tropospheric jet. For the suite of lower tropospheric heating and stratospheric cooling experiments, and $2\times\text{CO}_2$, the corresponding correlation is 0.92 in the NH and 0.91 in the SH. This is despite the fact that transient eddies should play a more important role in displacements of this jet. We also note that displacements of the surface wind correspond to those of the maximum Eady growth rate (Lindzen and Farrell, 1980). For example, the correlation between displacements of the maximum surface wind and the maximum 850 hPa Eady growth rate is 0.80 for the NH and 0.84 for the SH. Since the Eady growth rate is proportional to T_y , this is consistent

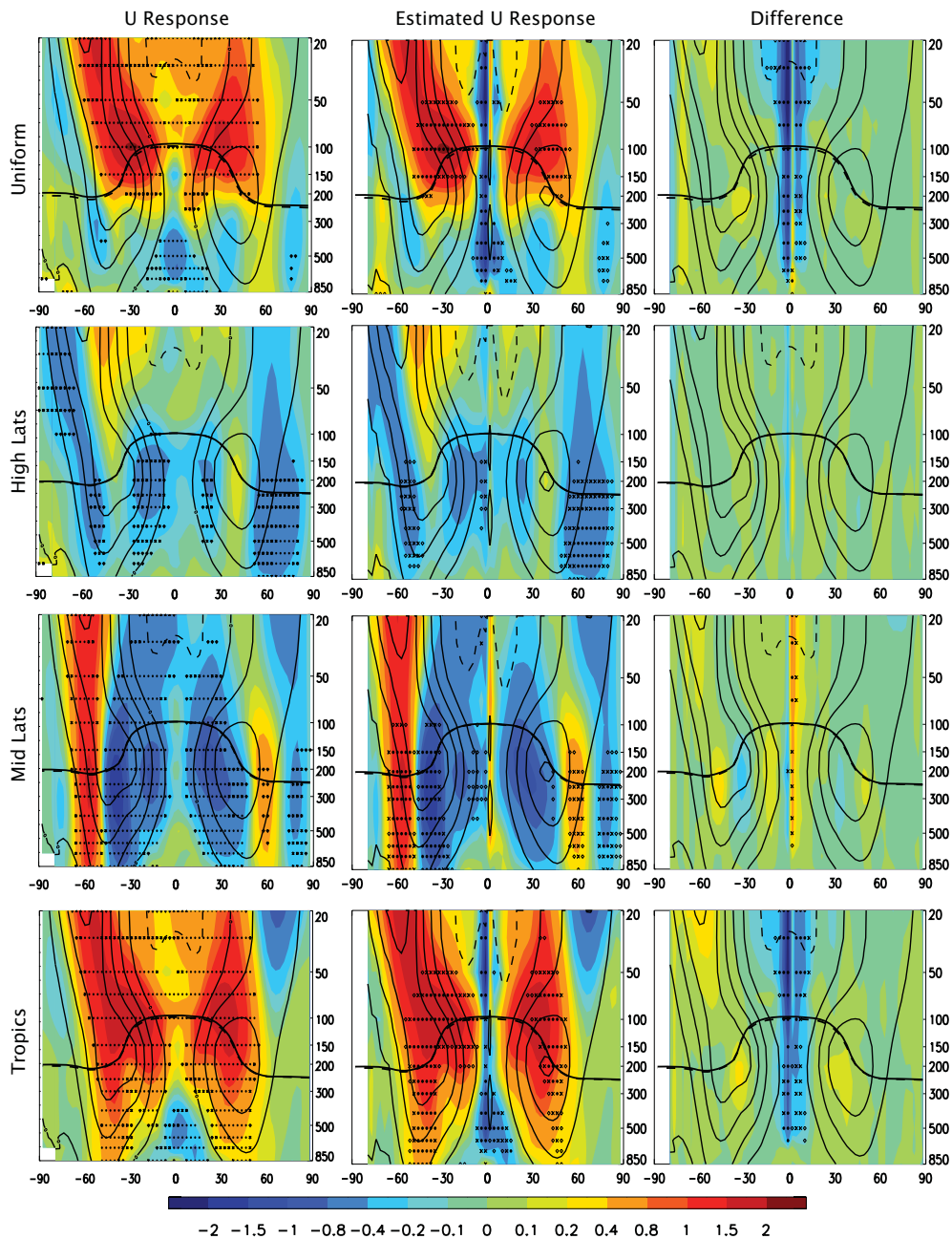


Fig. 5. Zonal annual mean zonal wind response (left), estimated zonal wind response (center) and difference (estimate-actual; right) for the lower-tropospheric heating experiments. The estimated U response is based on thermal wind balance, using the 900 hPa winds as a lower boundary condition. Also shown is the tropopause pressure for the (dashed) control and (solid) experiment. Symbols represent significance at the 90 % (diamond); 95 % (cross) and 99 % (dot) confidence level. Climatological U contour interval is 10 m s^{-1} with negative values dashed. Left panels (U response) are as in Fig. 3.

with our baroclinicity argument for tropospheric jet displacements and with the notion that storms tend to form in regions of high baroclinicity.

We note that the changes during El Niño events are consistent with our results. El Niño is associated with tropical tropospheric warming by warmer Pacific SSTs, mid-latitude tropospheric cooling due to eddy-driven upward motion, and

high-latitude tropospheric warming (Lu et al., 2008). The tropospheric jet, in turn, intensifies near the equatorward jet flank and weakens near the poleward flank, resulting in a strengthening and equatorward shift of the jet. The stronger jet is consistent with tropical warming and our LTHT_{TR} experiment. The equatorward shift is consistent with cooling in

the mid-latitudes and warming in the high-latitudes, as illustrated by our LTHT_{ML} and LTHT_{HL} experiments.

3.2.2 GFDL tropospheric heating experiments

To evaluate the robustness of the CAM responses to lower-tropospheric heating, we conducted analogous experiments with the GFDL AM2.1 (Anderson et al., 2004) using climatological SSTs. Figure 6 shows the corresponding annual mean temperature and zonal wind responses for $\text{LTHT}_{2\text{x}}$, $\text{LTHT}_{2\text{xTR}}$, $\text{LTHT}_{2\text{xML}}$, $\text{LTHT}_{2\text{xHL}}$. Results are similar to that based on CAM (Fig. 3). Heating of the tropics results in negligible jet displacement of -0.09° in the NH and -0.04° in the SH. However, high-latitude heating results in equatorward jet displacement (-0.26° in the NH and -0.10° in the SH) and mid-latitude heating results in poleward jet displacement of 0.75° in the NH (95 % significant) and 0.24° in the SH. The weaker GFDL response – particularly the SH response to mid-latitude heating – is likely due to the use of climatological SSTs, which mutes the tropospheric response. Repeating the GFDL mid-latitude heating experiment with double the heating rate (0.4 K day^{-1}) results in significant poleward jet displacement in both the NH and SH at 1.98° and 0.45° , respectively (not shown). We note that the main discrepancy between CAM and GFDL occurs for uniform heating of all latitudes. GFDL $\text{LTHT}_{2\text{x}}$ yields poleward jet displacement of 0.13° in the NH and 0.39° in the SH, the latter of which is significant at the 90 % confidence level. Although CAM $\text{LTHT}_{2\text{x}}$ yields similar, but weak, poleward jet displacement in the NH (0.12°), significant poleward jet displacement in the SH occurs (-0.73° ; Table 4).

3.2.3 Evidence of nonlinear responses

Table 4 shows that the LTHT responses are similar, but generally larger, when the heating rate is doubled ($\text{LTHT}_{2\text{x}}$). This includes tropical expansion for mid-latitude heating, tropical contraction for high-latitude heating, and negligible displacement for tropical heating. Unlike LTHT however, $\text{LTHT}_{2\text{x}}$ yields an “overall” equatorward jet displacement (NH + SH) of 0.61° , which is dominated by the SH jet which moves equatorward by 0.73° . Similarly, $\text{LTHT}_{4\text{x}}$ shows significant equatorward jet displacement of 1.46° , which again is dominated by the SH jet.

The bottom panel of Fig. 4 shows that the relationship between displacements of the maximum meridional tropospheric temperature gradient and the tropospheric jet also applies for the $\text{LTHT}_{2\text{x}}$ experiments. Note that as the heating rate is increased and the tendency for jet displacement is equatorward, the maximum T_y also shows a similar tendency of equatorward displacement. $\text{LTHT}_{4\text{x}}$, for example, shows significant equatorward displacement of the maximum T_y in both the SH and NH, in agreement with equatorward jet displacement (Table 4), particularly in the SH.

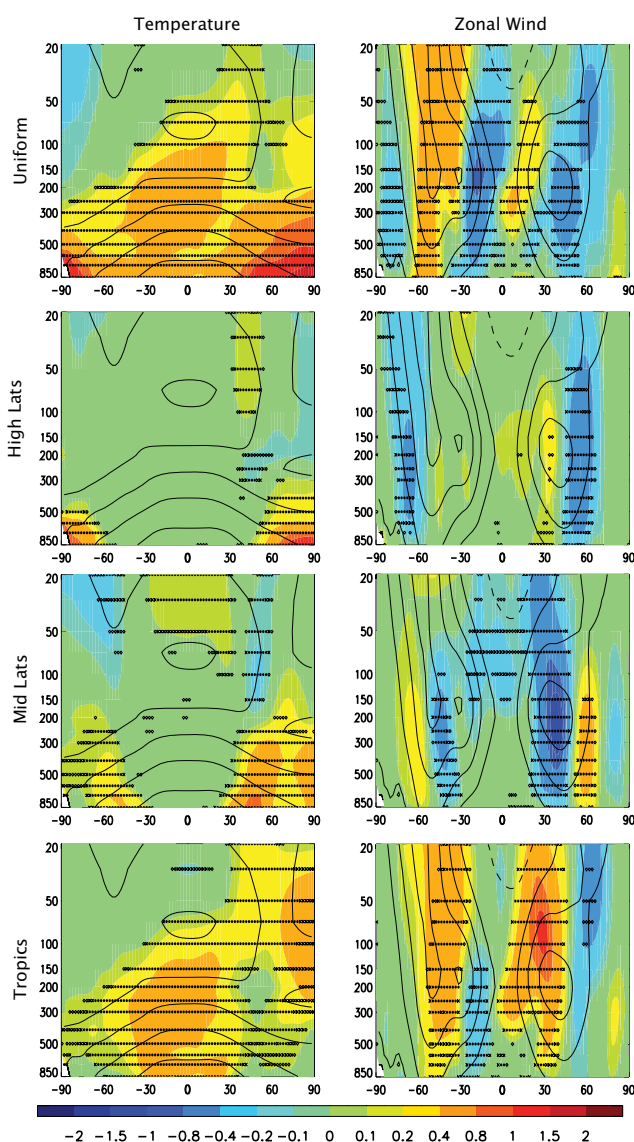


Fig. 6. Zonal annual mean temperature (left) and zonal wind (right) response to heating (0.2 K day^{-1}) the lower troposphere using the GFDL AM2.1 model. Symbols represent significance at the 90 % (diamond); 95 % (cross) and 99 % (dot) confidence level. Climatological U contour interval (thin black) with negative values dashed. Climatological T contour interval is 10 K .

One aspect of the uniform heating experiments that can be deduced from the above figures (e.g., Fig. 3) is that the responses are often nonlinear. For example, the sum of the poleward SH jet displacements in the LTHT_{TR} , LTHT_{ML} and LTHT_{HL} experiments is 0.77° , while the shift with uniform heating is smaller and in the opposite direction (-0.13°). This behavior recurs in the $\text{LTHT}_{2\text{x}}$ experiments, with values of 0.40° and -0.73° respectively. This nonlinear response is similar to the idealized experiments of Butler et al. (2010). This nonlinearity could be caused by the effects of localized heating on the vertical propagation of wave energy, and

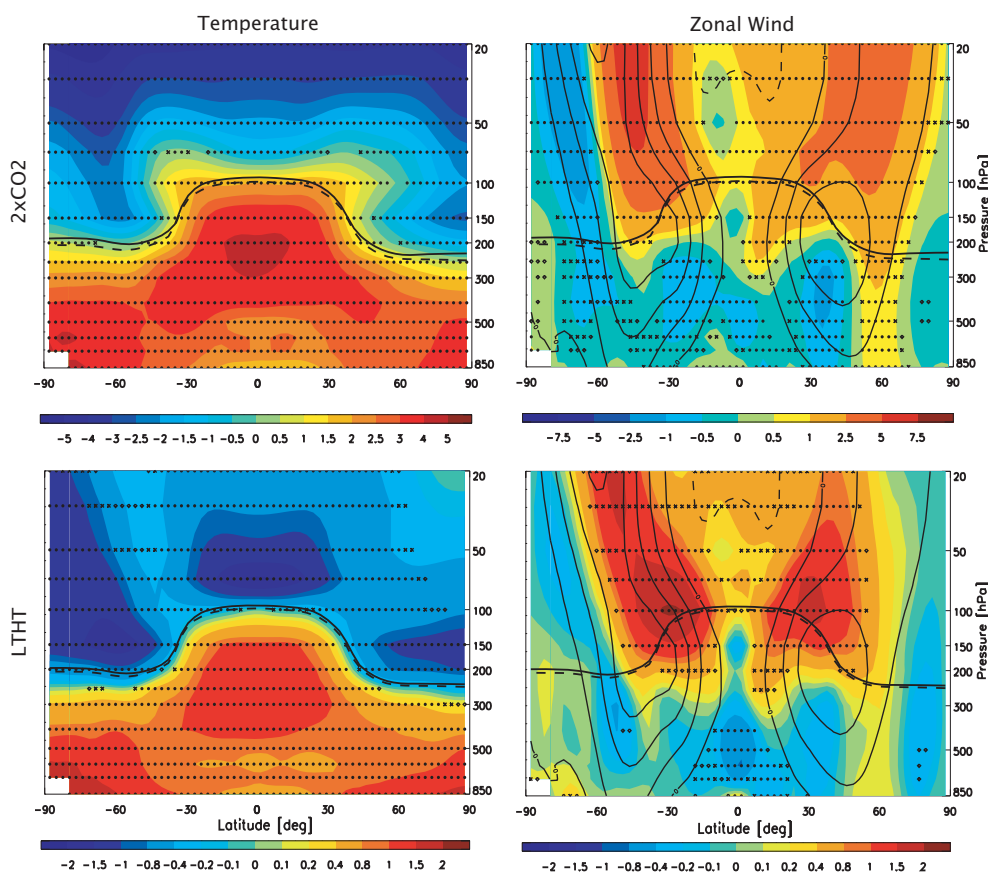


Fig. 7. $2\times\text{CO}_2$ (top) and LHHT (bottom) annual mean temperature (left) and zonal wind (right) response. LHHT results, and significance symbols, are as in Fig. 3. Note contour differences between $2\times\text{CO}_2$ and LHHT.

linear interference effects between the wave response and the background stationary wave (Smith et al., 2010; Fletcher and Kushner, 2011).

We note that the amplitude of jet displacement, however, appears to be more linear based on CMIP3 CO_2 experiments. Using the 10 $4\times\text{CO}_2$ CMIP3 models, we calculate the jet displacement using the 25 yr prior to doubling and the 25 yr prior to quadrupling (each compared to the corresponding control). For $4\times\text{CO}_2$, the ensemble annual mean NH jet displacement is 0.98° , compared to 0.35° for $2\times\text{CO}_2$; in the SH, the corresponding jet displacements are 1.74° and 0.81° , respectively. Thus, doubling the CO_2 forcing tends to yield double the jet displacement in CMIP3 experiments. This is similar to Wang et al. (2012), who found a linear relationship between the amplitude of the temperature response in the tropics and the tropospheric jet shift using a dry, idealized model (however, the eddy-driven jet exhibited an abrupt shift when tropical warming exceeded a critical amplitude).

Nearly all of the CAM heating experiments, as well as $2\times\text{CO}_2$, weaken the mean meridional circulation and strength of the tropospheric jet (not shown), in agreement with behavior of other GCMs and explainable by thermodynamic arguments (Held and Soden, 2006). LHHT_{TR}, how-

ever, strengthens the tropical circulation, with a 2 % increase in jet strength and a 4 % increase in mean meridional circulation strength. This strengthening increases to 5 % and 7 %, respectively, for LHHT $2X_{TR}$, so this particular result is relatively linear. These latitudinally restricted heating responses are consistent with Brayshaw et al. (2008).

3.3 Comparison of greenhouse gas warming and lower-tropospheric heating

Figure 7 shows the annual mean T and U response for LHHT and $2\times\text{CO}_2$. Both feature similar patterns of warming, with maximum warming in the tropical upper troposphere and at high-latitudes. Both also feature an increase in the height of the tropopause, as well as an upward displacement of the tropospheric jets (~ 10 hPa for $2\times\text{CO}_2$ and ~ 5 hPa for LHHT), which generally occurs with tropospheric heating (e.g., Lorenz and DeWeaver, 2007). The zonal jet displacement is also similar for the two experiments, with small SH displacements and larger NH poleward displacements, the latter of which is reminiscent of the positive NAM pattern. Note that the LHHT signal is much weaker than $2\times\text{CO}_2$. However, the global annual mean

surface temperature response for LTHT is also much weaker: 0.91 K versus 2.52 K for $2\times\text{CO}_2$.

Our experiments from Sect. 3.1 show that stratospheric cooling causes poleward jet displacement. Therefore, one reason why the LTHT experiments may yield less poleward jet displacement than those of $2\times\text{CO}_2$, is because $2\times\text{CO}_2$ is associated with significant stratospheric cooling due to increased longwave emission to space; LTHT, however, has no directly imposed stratospheric cooling (although there is an indirect stratospheric cooling response). This was evaluated by rerunning the LTHT, LTHT $2x$ and LTHT $4x$ experiments, but with a 10% stratospheric ozone reduction (LTHT $_{10\text{PLO}_3}$, LTHT $2x_{10\text{PLO}_3}$, LTHT $4x_{10\text{PLO}_3}$). For both LTHT $2x$ and LTHT $4x$, adding stratospheric cooling yields less equatorward jet displacement, particularly the SH jet for LTHT $2x$, but the differences are generally not large (Table 5)). This suggests that the tropospheric warming is more important than the stratospheric cooling.

4 Discussion of expansion scenarios

Prior studies have attributed tropical expansion in a warmer climate to increases in the tropopause height (e.g., Lorenz and DeWeaver, 2007; Williams, 2006) and/or extratropical dry static stability (e.g., Frierson et al., 2007; Lu et al., 2007). Figure 8 shows the changes in these two quantities, in addition to the 500 hPa T_y change and its climatology for four of the tropospheric heating experiments. These four experiments were chosen because they allow the evaluation of these previously proposed mechanisms. The top two panels compare the response based on heating of the mid-latitudes in either the lower (LTHT $_{\text{ML}}$) or upper (UTHT $_{\text{ML}}$) troposphere. Of the two, the latter results in a larger increase in gross dry static stability of mid-latitudes, as expected. Although both experiments yield poleward jet displacement, tropical expansion is generally larger with LTHT $_{\text{ML}}$. Table 4 shows this is particularly true in the SH, where the annual mean jet displacement is 1.02° for LTHT $_{\text{ML}}$ versus 0.53° for UTHT $_{\text{ML}}$. Similar conclusions exist based on the other metrics of tropical expansion (Table 5), particularly $P - E$. The larger LTHT $_{\text{ML}}$ poleward jet displacement is inconsistent with a smaller increase in stability; however, it is consistent with thermal wind balance and a larger poleward displacement of the 500 hPa SH T_y .

The bottom two panels show that heating of the high-latitudes and tropics results in an increase in tropopause height (decrease in pressure), yet neither experiment is associated with tropical expansion. LTHT $2x_{\text{HL}}$ actually yields significant equatorward jet displacement of -0.74° (-0.32° and -0.42° for NH and SH, respectively) and LTHT $2x_{\text{TR}}$ yields negligible jet displacement of -0.23° (Table 4). These responses are again consistent with the change in T_y at 500 hPa, with a weakening of T_y at high latitudes for LTHT $2x_{\text{HL}}$, and a reinforcement of the climatological T_y for

LTHT $2x_{\text{TR}}$. These results suggest the importance of other mechanisms in driving jet displacements, at least using CAM under our experimental design.

4.1 Stratospheric pathway

Section 3.1 showed cooling of the high-latitude stratosphere resulted in poleward jet displacement. Table 4 shows the largest NH jet displacements in response to stratospheric cooling occur during March–April–May (MAM), and the equivalent season in the SH (SON) similarly shows the largest response in its jet. The maximum spring response is likely due to a combination of two factors: the presence of solar radiation, so that the imposed ozone loss results in stratospheric cooling; and westerly stratospheric flow, which is conducive to strong planetary wave–mean flow interaction. The cooling of the high-latitude stratosphere increases the local meridional temperature gradient, and the stratospheric vortices in both hemispheres intensify in accord with thermal wind balance. The downward propagation of the stratospheric wind anomaly may be related to enhanced equatorward refraction of Rossby waves (Shindell et al., 2001; Rind et al., 2005). As a diagnostic tool to estimate the importance of this “stratospheric pathway”, we estimate the wave refraction (λ) as the ratio of meridional to vertical Eliassen Palm (EP) flux:

$$\lambda = \frac{-\overline{u^*v^*}}{f R_d \overline{v^*T^*} / N^2 H}, \quad (1)$$

where $\overline{u^*v^*}$ is the meridional eddy momentum flux, $\overline{v^*T^*}$ is the meridional eddy heat flux, N is the Brunt–Vaisala frequency, R_d is the dry air gas constant, H is the scale height, f is the Coriolis parameter and primes denote a zonal deviation. Because both eddy fluxes are estimated from monthly data, λ represents the refraction of the quasi-stationary, as opposed to the transient, waves.

Table 6 shows that all stratospheric cooling experiments feature an increase in MAM NH wave refraction by 15–35% – the season of maximum poleward jet displacement in the NH. Figure 9 shows the MAM responses of T , U and T_y for one stratospheric cooling experiment, $10\text{PLO}_3_{\text{HL}}$. Also included is the leading pattern of zonal wind anomalies, and the mean meridional circulation, associated with the NAM/SAM pattern. This pattern is based on a principal component analysis of geopotential heights for the domains extending from $20\text{--}90^\circ$ N/S and from 1000 to 10 hPa. Data are weighted by the square root of the cosine of the latitude, as well as by the square root of the pressure interval represented by that level (Thompson and Wallace, 2000). The wind fields are then regressed upon the resulting standardized leading principal component (PC) time series.

The changes in zonal wind and mean meridional circulation closely resembles the NAM (and to a lesser extent, the SAM) pattern, which suggests the response may involve

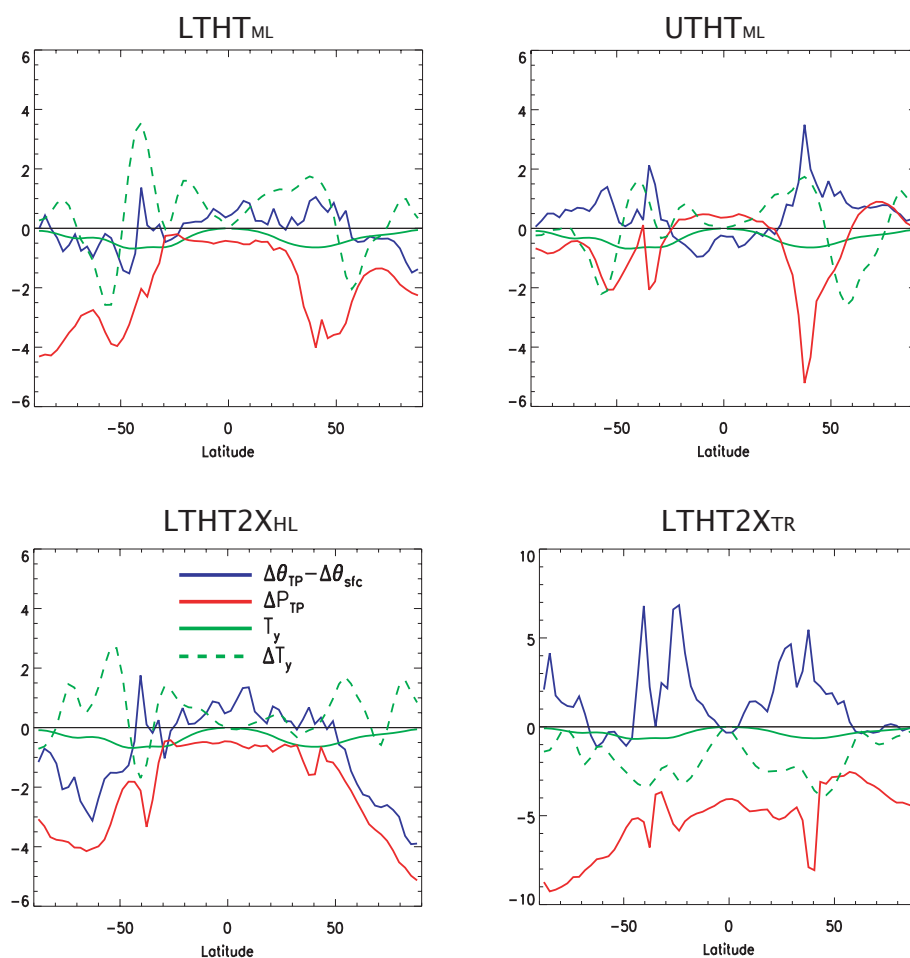


Fig. 8. Annual mean gross dry static stability change (blue; $\Delta\theta_{TP} - \Delta\theta_{sfc}$), tropopause pressure change (red; ΔP_{TP}), climatological baroclinicity at 500 hPa (green solid; T_y) and the corresponding response (green dashed; ΔT_y) for (top left) $LTHT_{ML}$, (top right) $UTHT_{ML}$, (bottom left) $LTHT2x_{HL}$ and (bottom right) $LTHT2x_{TR}$. Units are K, hPa, $K km^{-1} 10^{-4}$ and $K km^{-1} 10^{-2}$, respectively.

wave mean-flow interaction and downward control theory (Haynes et al., 1991; Baldwin and Dunkerton, 1999). The MAM 10PLO3_{HL} response also features an anomalous tropospheric meridional circulation, with rising motion poleward of 60°, sinking motion between 30–60°, and equatorward flow in the upper troposphere, somewhat like an intensified Ferrel Cell, but stretched poleward. This thermally indirect circulation coincides with warming near its sinking branch (near 45°), and cooling in the rising branch (near 70°). Imposition of these temperature anomalies on the background state produces a poleward displacement of the maximum tropospheric T_y , consistent with the tropospheric zonal wind anomaly near 60°. Figure 9 suggests that this anomalous residual circulation – particularly in the NH – is balanced by a poleward shift of eddy westerly momentum flux convergence near 60°, which sustains the westerly wind anomaly. The response is also associated with an increase in downward, equatorward wave energy and EP-flux divergence in the mid-latitude stratosphere and troposphere.

We find that our analysis of the NH spring-time response also approximately holds for the SH (not shown). For example, each stratospheric cooling experiment features an increase in SH SON wave refraction: 23 %, 21 %, 32 % and 2 % for 10PLO3, 10PLO3_{HL}, 10PLO3_{ML} and 10PLO3_{TR}, respectively.

For $2\times CO_2$ and LTHT, Table 4 shows NH tropical expansion primarily occurs during two seasons: MAM and DJF. Similar to the stratospheric cooling experiment, both LTHT and $2\times CO_2$ feature a NAM-like U response and meridional circulation response pattern, which is associated with a wave-modulated stratospheric pathway (not shown). Both signals feature an increase in wave refraction (Table 6), which is associated with an increase in downward, equatorward wave energy and EP-flux divergence in the mid-latitude stratosphere and troposphere. An anomalous meridional circulation in the troposphere and a poleward shift of eddy westerly momentum flux convergence near 60° N, also occurs. Similarly, CMIP3 $2\times CO_2$ also features an increase in NH MAM

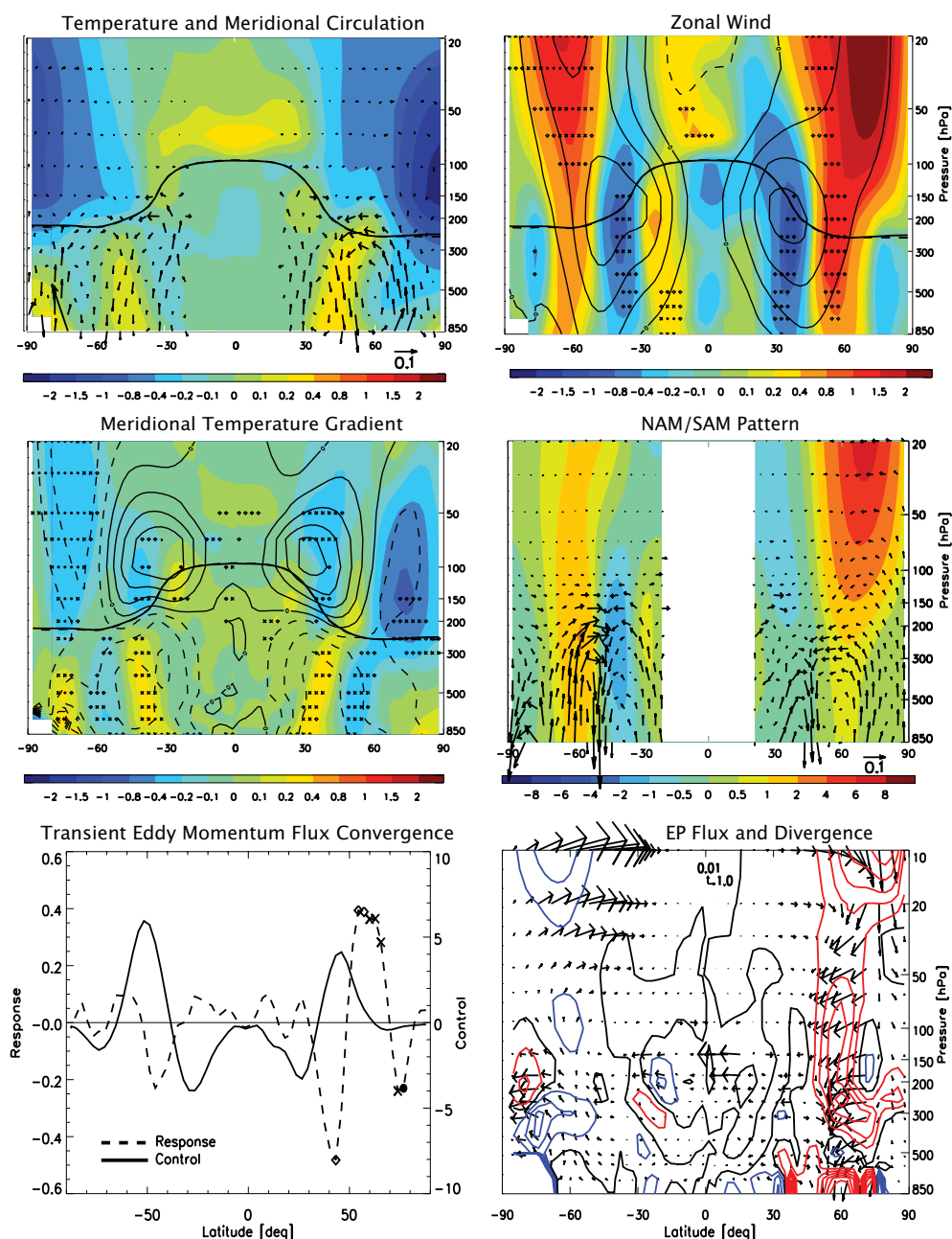


Fig. 9. MAM 10PLO3_{HL} response of (top left) temperature and meridional circulation, (top right) zonal wind, (middle left) meridional temperature gradient, (middle right) SAM/NAM U pattern, (bottom left) 250 hPa transient eddy momentum flux convergence [K m s^{-1}] and (bottom right) EP flux [$\text{m}^2 \text{s}^{-2}$] and flux divergence [10^{-6} m s^{-2}], divided by the standard density. T_y (U) contour interval is $2 \times 10^{-3} \text{ K km}^{-1}$ (10 m s^{-1}) with negative values dashed. Units of NAM/SAM are m s^{-1} per standard deviation of the PC time series. Indicated vector length (top left) represents 0.1 cm s^{-1} for the meridional component and $-0.1 \times 10^{-4} \text{ Pa s}^{-1}$ for the vertical component. EP flux divergence contour interval is $[-6, -5, -4, -3, -2, -1, 0, 1, 2, 3, 4, 5, 6]$, with negative values blue and positive values red. Symbols represent significance as in Fig. 2. Transient eddy momentum flux, $\overline{u'v'}$ is estimated according to $\overline{uv} - \bar{u}\bar{v}$, where primes denote zonal deviations and overbars indicate zonal averages.

and DJF wave refraction of 15 % and 13 %, respectively (Table 6). Moreover, a significant, but weak, relationship exists between CMIP3 $2 \times \text{CO}_2$ NH wave refraction and jet displacement for both DJF and MAM, with correlations of 0.44

and 0.43, respectively. This suggests that a wave-modulated stratospheric pathway may play an important role in warming induced tropical expansion, particularly in the NH during MAM and DJF, regardless of the cause of the warming.

Table 6. Northern Hemisphere 850–20 hPa percent change in wave refraction for the (top) stratospheric cooling experiments and (bottom) global warming experiments. Also included is the mid-latitude, lower tropospheric heating experiments (LTHT_{ML} and LTHT2_{xML}), as well as the ensemble mean CMIP3 2×CO₂ wave refraction. Wave refraction is estimated as the meridional component of EP flux divided by the vertical component. A more positive value indicates more equatorward wave propagation.

Signal	DJF	MAM	JJA	SON
10PLO3	2	15	−26	5
10PLO3 _{HL}	1	35	−25	−8
10PLO3 _{ML}	21	25	−8	−2
10PLO3 _{TR}	5	20	−29	−8
LTHT	19	21	−25	−3
LTHT2 _x	23	38	−22	−7
LTHT4 _x	26	−32	−31	−17
2×CO ₂	33	56	−12	4
8×CO ₂	49	49	38	15
LTHT _{ML}	3	8	−13	−8
LTHT2 _{xML}	39	12	−16	2
2×CO ₂ CMIP3	13	15	−13	24

We also note that similar behavior occurs for the mid-latitude lower-tropospheric heating experiments. Both LTHT_{ML} and LTHT2_{xML} feature an increase in MAM downward, equatorward wave energy (increase in wave refraction, Table 6) and EP-flux divergence, as well as cooling of the polar stratosphere, a decrease in polar stratospheric geopotential heights and a decrease in high-latitude surface pressure (not shown). This is analogous (but opposite) to the negative NAM response to anomalous Eurasian snow cover (e.g., Cohen et al., 2007; Fletcher et al., 2009; Allen and Zender, 2010).

4.2 Tropospheric pathway

Figure 10 shows a scatterplot of the tropospheric (850–300 hPa) jet displacement versus the difference in mid- and high-latitude warming amplification for the 5 global warming experiments (LTHT, LTHT2_x, LTHT4_x, 2×CO₂ and 8×CO₂) and 6 latitude-restricted heating experiments (LTHT_{TR}, LTHT_{ML}, LTHT_{HL}, LTHT2_{xTR}, LTHT2_{xML}, LTHT2_{xHL}). Warming amplification of mid-latitudes (AMP_{ML}) is defined as the log-pressure area weighted temperature (i.e., thickness) response between 30–60° minus that between 0–30°. For high-latitudes (AMP_{HL}), the log-pressure area weighted temperature response between 60–90° is differenced with that between 30–60°. Table 7 lists the amplification factors. This choice of this metric was inspired by the responses found in the latitude-restricted tropospheric heating experiments. When high-latitudes warm relative to mid-latitudes, AMP_{HL} is positive, and we expect equatorward jet displacement. When

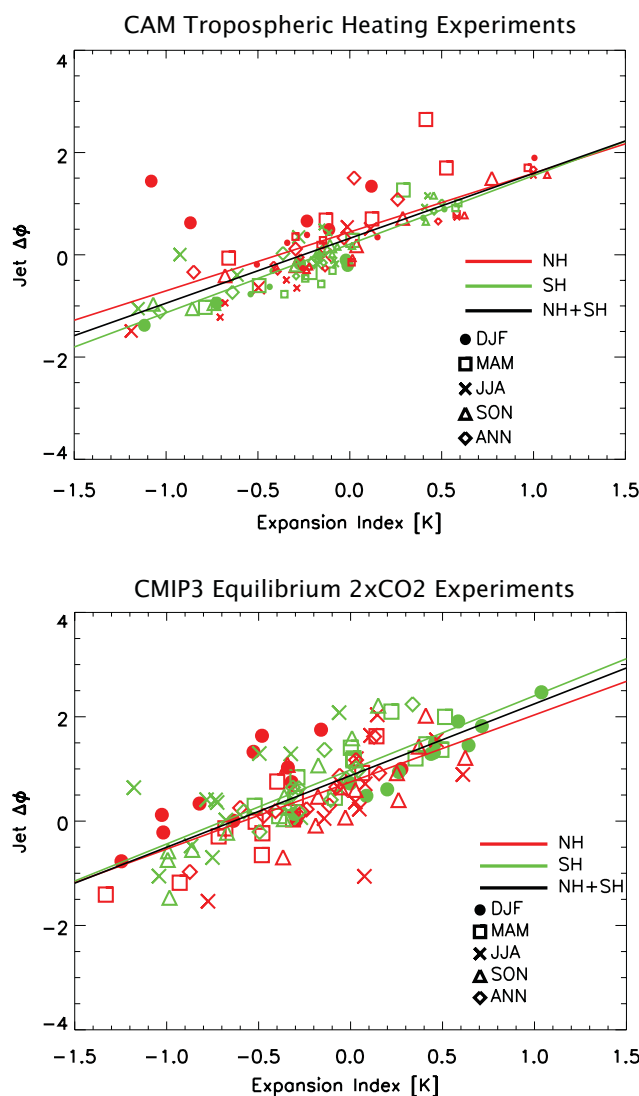


Fig. 10. Scatterplot of tropospheric poleward jet displacement versus the expansion index for the (top panel) CAM tropospheric heating experiments and (bottom panel) 12 CMIP3 2×CO₂ equilibrium experiments. CAM tropospheric heating experiments include the 5 global warming experiments (larger symbols; LTHT, LTHT2_x, LTHT4_x, 2×CO₂, 8×CO₂) and 6 latitude-restricted heating experiments (smaller symbols; LTHT_{TR}, LTHT_{ML}, LTHT_{HL}, LTHT2_{xTR}, LTHT2_{xML}, LTHT2_{xHL}). Also included are the corresponding linear regression lines, all of which are significant at the 99 % confidence level.

the mid-latitudes warm relative to low-latitudes, AMP_{ML} is positive, and we expect poleward jet displacement. Taking the difference, AMP_{ML} − AMP_{HL}, results in a quantity that accounts for these two competing effects. As the difference becomes more positive/less negative, then mid-latitude warming amplification dominates, and we expect more tropical expansion/less contraction; vice versa as AMP_{ML} − AMP_{HL} becomes less positive/more negative. We call this quantity the “Expansion Index” (EI). Based on

Table 7. Tropospheric (850–300 hPa) warming amplification factors for high-latitudes (HL; 60–90° minus 30–60°) and mid-latitudes (ML; 30–60° minus 0–30°) for the global warming experiments. Factors are based on log-pressure and area weighting. Also included are the corresponding values based on the ensemble mean of 12 CMIP3 2×CO₂ experiments. Units are K.

Signal	ANN		DJF		MAM		JJA		SON		
	HL	ML	HL	ML	HL	ML	HL	ML	HL	ML	
LTHT	NH	0.02	−0.01	−0.01	−0.13	−0.14	−0.02	0.22	0.08	−0.02	0.02
	SH	0.22	0.03	0.24	−0.04	0.27	0.05	0.23	0.05	0.16	0.05
LTHT2x	NH	0.16	−0.13	−0.06	−0.29	0.01	−0.12	0.41	−0.08	0.24	−0.04
	SH	0.62	−0.02	0.62	−0.11	0.56	0.07	0.63	0.02	0.67	−0.07
LTHT4x	NH	0.64	−0.21	0.40	−0.47	0.35	−0.30	1.15	−0.03	0.66	−0.02
	SH	1.02	−0.01	0.94	−0.17	0.93	0.15	1.18	0.03	1.03	−0.03
2×CO ₂	NH	−0.05	0.21	−0.15	−0.03	−0.37	0.16	0.24	0.35	0.07	0.36
	SH	0.36	0.22	0.29	0.27	0.30	0.31	0.45	0.17	0.43	0.13
8×CO ₂	NH	1.08	1.10	1.04	−0.03	0.10	0.52	2.11	2.10	1.05	1.82
	SH	0.95	0.59	0.63	0.61	0.70	1.00	1.35	0.43	1.15	0.29
2×CO ₂ CMIP3	NH	0.03	−0.40	0.14	−0.40	0.10	−0.39	−0.07	−0.02	−0.05	0.02
	SH	−0.23	−0.41	−0.59	−0.21	−0.35	−0.29	0.10	−0.56	−0.08	−0.57

the 6 latitude-restricted heating experiments in Fig. 10, EI accounts for 86 % of the NH and SH jet displacements. For the annual mean only, EI accounts for 94 % of the NH and SH jet displacements. We note that EI can be rewritten as the difference between twice the mid-latitude warming and the sum of low- and high-latitude warming (a rough Laplacian): $2 \times \Delta T_{30-60} - (\Delta T_{0-30} + \Delta T_{60-90})$.

The global warming experiments are generally consistent with this notion. Over all five experiments and seasons, the relationship is significant at the 99 % confidence level for NH, SH and both hemispheres, accounting for 42 %, 72 % and 55 % of the jet displacement, respectively. For the annual mean only, the expansion index accounts for 76 % of the NH and SH jet displacement. The dominant response in these experiments – equatorward SH jet displacement – is consistent with the large SH high-latitude warming, and large AMP_{HL}. The diagnostic also explains the increased equatorward displacement when the heating rate is increased in the LTHT experiments. Increasing the heating rate generally results in amplified high-latitude warming, which is associated with equatorward jet displacement. Table 7 shows that the annual mean SH AMP_{HL} increases from 0.22 to 1.02 K for LTHT to LTHT4x; and from 0.02 to 0.64 K in the NH. At the same time, however, AMP_{ML} generally decreases, particularly in the NH. Furthermore, AMP_{HL} is generally largest in the SH, relative to the NH, consistent with equatorward SH jet displacement in nearly all cases. The relationship is weakest in the NH for DJF and MAM, which may be related to the wave-modulated stratospheric pathway during these seasons. Without DJF and MAM, the expansion index accounts for 81 % of the variation in NH jet displacement. Similar conclusions exist when the three mid-tropospheric global warming

experiments (MTHT, MTHT2x and MTHT4x) are included in the analysis.

Figure 10 further supports the idea that part of the jet shift can be thought of as a geostrophic adjustment to an altered temperature profile – not only when certain latitude bands are heated, but also for global warming experiments like LTHT and 2×CO₂. Our experiments suggest that poleward jet displacement is partially driven by mid-latitude heating, while equatorward jet displacement is partially driven by high-latitude heating. However, a wave-modulated stratospheric pathway during the NH active seasons is also important, resulting in poleward NH jet displacement during MAM and DJF which projects onto the positive phase of the NAM. For LTHT this mechanism eventually weakens with increased heating (e.g., LTHT4x), where high-latitude amplification dominates and the maximum T_y is displaced equatorward, resulting in equatorward displacement of the tropospheric jets.

Figure 10 also shows a similar relationship between the expansion index and jet displacement exist based on CMIP3 2×CO₂ equilibrium experiments. Even though this metric does not directly account for the effects of CO₂ induced stratospheric cooling, it accounts for 45 %, 67 % and 56 % of the of the variation in jet displacement in the NH, SH and both hemispheres, respectively. Based on the annual mean only, EI accounts for 76 % of the NH and SH jet displacement. Similar results are obtained if jet displacements are based on others percentiles. Using the 70th–95th percentile in 5 percentile increments, EI accounts for 61 % to 77 % of the annual mean jet displacement; using the alternate, maximum U method, 66 % of the annual mean jet displacement is accounted for. This relationship is somewhat better than the relationship Lu et al. (2007) found between tropical

expansion and tropopause height (stability); there, increases in extratropical (35–55°) tropopause height accounted for 66 % of the variation in annual mean MMC expansion using CMIP3 A2 experiments. More recently, Lu et al. (2008) found a significant relationship between poleward MMC displacement and a decrease in Philips criticality, the latter of which occurred primarily due to an increase in extratropical static stability. In the SH during DJF, Philips criticality accounted for 67 % of the variation in MMC expansion. Similarly, the expansion index accounts for 92 % of the jet displacement in the SH during DJF. We also find that it accounts for most of the DJF SH variation in other metrics of tropical expansion, including $P - E$ (81 %) and MMC (81 %). Similar, but weaker, results exist for SH ANN, where the expansion index accounts for 45 % and 46 % of the variation in $P - E$ and MMC, respectively. Thus, the expansion index helps to explain not only dynamical measures of tropical expansion, but hydrological measures too, particularly in the SH.

We also estimated the relationship between the expansion index and tropospheric jet displacement using the 10 1 % to 4×CO₂ CMIP3 experiments, and with five reanalyses, including NCEP/NCAR (Kalnay et al., 1996), NCEP-DOE (Kanamitsu et al., 2002), MERRA (Rienecker et al., 2011), ERA40 (Uppala et al., 2005) and ERA-Interim (Dee et al., 2011). The first three reanalyses are analyzed from 1979–2010; ERA40 from 1979–2002 and ERA-Interim from 1989–2010. Based on the annual mean, the expansion index accounts for 70 % of the variance in NH and SH jet displacements in 4×CO₂ CMIP3 experiments; and 55 % of the corresponding jet displacements in reanalyses.

We conclude by comparing the CAM global warming experiments with the CMIP3 2×CO₂ experiments. Similar to the CAM experiments, the EI-jet displacement relationship is weakest in the NH during DJF, where it accounts for only 46 % of the variation in jet displacement. We also note that the NH MAM CAM 2×CO₂ jet displacement is much larger than the CMIP3 ensemble (1.70° versus −0.01°), which is consistent with more MAM wave refraction in CAM 2×CO₂ (56 % versus the CMIP3 ensemble mean of 15 %). CAM 2×CO₂ also features less SH jet displacement than CMIP3 (0.09° versus 0.73° for the annual mean), despite a similar expansion index (−0.14 versus −0.18 for CMIP3). Although the reasons are not clear, the other metrics of CAM 2×CO₂ tropical width both show greater SH displacement (0.60° for $P - E$ and 0.42° for MMC). In addition to these equilibrium experiments, we have also conducted transient CO₂ CAM experiments over the latter half of the 20th century using several ensembles (not shown) and obtain similar minimal SH jet displacement. This suggests CAM3 is less sensitive to CO₂-induced SH poleward jet displacement, relative to other CMIP3 models.

5 Conclusions

The CAM3 general circulation model is used to investigate how tropical width responds to idealized thermal perturbations, focusing on zonal displacement of the tropospheric jets. The heat sources include global and zonally restricted lower-tropospheric warmings and stratospheric coolings, which coarsely represent possible impacts of ozone or aerosol changes. Our results show that global stratospheric cooling, as well as stratospheric cooling of the high- and mid-latitudes, yields poleward jet displacement. This response is related to wave-mean flow interaction and involves an increase in wave refraction, and downward propagation of the stratospheric wind anomaly. This response is in general agreement with similar studies using idealized models (e.g., Haigh et al., 2005) and supports the recent findings of Polvani et al. (2011), who showed stratospheric ozone loss is the main driver of twentieth century atmospheric circulation changes in the Southern Hemisphere (SH).

CAM3 tropospheric heating experiments show that high-latitude heating results in equatorward jet displacement; mid-latitude heating results in poleward jet displacement; and low-latitude heating yields negligible jet displacement (but a significant increase in the strength of the tropical circulation). Similar results were obtained with the GFDL AM2.1. Although our high-latitude response is consistent with a recent study using a simplified GCM (Butler et al., 2010), our tropical heating results differ – Butler et al. (2010) found tropical heating forces a significant poleward shift of the extratropical storm tracks (and tropospheric jets). We note that the Butler et al. (2010) results appear to contradict the El Niño response, which is associated with tropical tropospheric warming and equatorward displacement of the jets (Lu et al., 2008). Reasons for this discrepancy are unclear, but may be related to the meridional extent of the forcing and subsequent temperature response. The tropical heating in Butler et al. (2010) extends all the way to 45° N/S, whereas our LTHT_{TR} heating extends to 30° N/S. As noted in Butler et al. (2010), the projection of this heating into the mid-latitudes may play a significant role in the jet shift. Perhaps a more appropriate comparison to their tropical heating experiment is our LTHT_{TRML} experiment, where heat is added from 0–60° N/S. Similar to the Butler et al. (2010) result, LTHT_{TRML} yields mid-latitude warming and poleward jet displacement. Additional possibilities for the discrepancy are the existence of topography in our model, which is important for the wave-modulated stratospheric pathway; and moisture/convective processes which could change the way heat is distributed.

Globally uniform lower tropospheric heating (LTHT) and 2×CO₂ yield similar tropical width responses. Both yield negligible jet displacement in the SH and poleward jet displacement in the NH, particularly during DJF and MAM. Similar to the stratospheric cooling experiments, the boreal winter/spring expansion is related to a wave-modulated stratospheric pathway and a positive NAM-like response.

This result is consistent with Previdi and Liepert (2007), who showed 50 % of the subtropical dry zone expansion can be explained by positive trends in the annular modes. Other metrics of tropical displacement, including $P - E$ and MMC, generally yield a similar response. However, there are some differences that warrant further study.

Jet shifts associated with the tropospheric heating experiments are related to zonal displacements of the maximum meridional tropospheric temperature gradient. Heating the mid-latitudes results in maximum mid-latitude warming, consistent with a down gradient eddy heat flux response (i.e., oriented away from the latitude of maximum heating). This weakens the tropospheric meridional temperature gradient (T_y) on the equatorward flank of the T_y maximum and strengthens T_y on the poleward flank of the maximum. The jet responds by moving poleward, consistent with a geostrophic adjustment to the altered meridional temperature gradient, in accord with thermal wind balance. The opposite occurs when heat is added to the high-latitudes. This relationship also exists for global warming experiments, including LHTT and $2 \times \text{CO}_2$.

Some of our experiments are inconsistent with previously proposed mechanisms of tropical expansion (e.g., Lorenz and DeWeaver, 2007; Frierson et al., 2007; Lu et al., 2007). For example, heating the tropical troposphere results in a global increase in tropopause height, yet negligible poleward tropical displacement. Our experiments highlight the importance of altered tropospheric temperature gradients and a wave-modulated stratospheric pathway. For the global warming experiments, the “Expansion Index”, which quantifies the difference between mid-latitude and high-latitude warming amplification, accounts for over half of the tropospheric jet displacements; this increases to over 70 % for annual mean jet displacements. A similar relationship also exists for $2 \times \text{CO}_2$ CMIP3 equilibrium experiments and 1 % to $4 \times \text{CO}_2$ CMIP3 transient experiments. Five reanalyses also show the relationship exists for recent climate trends.

This study has important implications for heterogeneous warming agents, such as tropospheric ozone and absorbing aerosols, as briefly discussed by Allen and Sherwood (2011). Such non- CO_2 forcings – particularly those that warm the mid-latitudes and are underestimated by most models (e.g., Ramanathan and Carmichael, 2008; Koch et al., 2009) – may help explain the discrepancy between modeled and observed estimates of recent tropical expansion. Moreover, a recent study by Scaife et al. (2012) found increased CO_2 in GCMs with a well-resolved stratosphere yielded an equatorward storm track shift, particularly over the Atlantic during winter. This implies the observed poleward shift may be due more to heterogeneous warming agents, as opposed to greenhouse gases. We are currently investigating the importance of non- CO_2 forcings in recent tropical expansion.

Acknowledgements. This study was funded by RJA’s UCR initial complement, SIO NOAA grant NA10OAR43210141, and by NSF ARC-0714088 and NASA NNX07AR23G, UC Irvine. We acknowledge the modeling groups, the Program for Climate Model Diagnosis and Intercomparison (PCMDI) and the WCRP’s Working Group on Coupled Modelling (WGCM) for their roles in making available the WCRP CMIP3 multi-model dataset. Support of this dataset is provided by the Office of Science, US Department of Energy. We thank Amy Butler, and one anonymous reviewer, for their helpful comments.

Edited by: T. J. Dunkerton

References

- Allen, R. J. and Sherwood, S. C.: The impact of natural versus anthropogenic aerosols on atmospheric circulation in the Community Atmosphere Model, *Climate Dyn.*, 36, 1959–1978, doi:10.1007/s00382-010-0898-8, 2011.
- Allen, R. J. and Zender, C. S.: The effects of continental-scale snow albedo anomalies on the wintertime Arctic Oscillation, *J. Geophys. Res.*, 115, D23105, doi:10.1029/2010JD014490, 2010.
- Anderson, J., Balaji, V., Broccoli, A., Cooke, W., Delworth, T., Dixon, K., Donner, L., Dunne, K., Freidenreich, S., Garner, S., Gudgel, R., Gordon, C., Held, I., Hemler, R., Horowitz, L., Klein, S., Knutson, T., Kushner, P., Langenhost, A., Lau, N., Liang, Z., Malyshev, S., Milly, P., Nath, M., Ploshay, J., Ramaswamy, V., Schwarzkopf, M., Shevliakova, E., Sirutis, J., Soden, B., Stern, W., Thompson, L., Wilson, R., Wittenberg, A., Wyman, B., and GFDL Global Atmospheric Model Dev: The new GFDL global atmosphere and land model AM2-LM2: Evaluation with prescribed SST simulations, *J. Climate*, 17, 4641–4673, 2004.
- Baldwin, M. P. and Dunkerton, T. J.: Propagation of the Arctic Oscillation from the stratosphere to the troposphere, *J. Geophys. Res.*, 104, 30937–30946, 1999.
- Bond, T. C., Bhardwaj, E., Dong, R., Jogani, R., Jung, S., Roden, C., Streets, D. G., and Trautmann, N. M.: Historical emissions of black and organic carbon aerosol from energy related combustion, 1850–2000, *Global Biogeochem. Cy.*, 21, GB2018, doi:10.1029/2006GB002840, 2007.
- Brayshaw, D. J., Hoskins, B., and Blackburn, M.: The storm-track response to idealized SST perturbations in an aquaplanet GCM, *J. Atmos. Sci.*, 65, 2842–2860, 2008.
- Butler, A. H., Thompson, D. W. J., and Heikes, R.: The steady-state atmospheric circulation response to climate change-like thermal forcings in a simple general circulation model, *J. Climate*, 23, 3474–3496, 2010.
- Butler, A. H., Thompson, D. W. J., and Birner, T.: Isentropic slopes, downgradient eddy fluxes, and the extratropical atmospheric circulation response to tropical tropospheric heating, *J. Atmos. Sci.*, 68, 2292–2305, 2011.
- Chen, G. and Held, I.: Phase speed spectra and the recent poleward shift of the Southern Hemisphere surface westerlies, *Geophys. Res. Lett.*, 34, L21805, doi:10.1029/2007GL031200, 2007.
- Chen, G., Lu, J., and Frierson, D. W.: Phase speed spectra and the latitude of surface westerlies: Interannual variability and global warming trend, *J. Climate*, 21, 5942–5959, 2008.
- Chen, G., Plumb, R. A., and Lu, J.: Sensitivities of zonal mean atmospheric circulation to SST warming in an aqua-planet model,

- Geophys. Res. Lett., 37, L12701, doi:10.1029/2010GL043473, 2010.
- Chung, C. E., Ramanathan, V., Kim, D., and Podgorny, I. A.: Global anthropogenic aerosol direct forcing derived from satellite and ground-based observations, *J. Geophys. Res.*, 110, D24207, doi:10.1029/2005JD006356, 2005.
- Cohen, J., Barlow, M., Kushner, P. J., and Saito, K.: Stratosphere-troposphere coupling and links with Eurasian land surface variability, *J. Climate*, 20, 5335–5343, 2007.
- Collins, W. D., Rasch, P. J., Boville, B. A., Hack, J. J., McCaa, J. R., Williamson, D. L., Kiehl, J. T., Briegleb, B., Bitz, C., Lin, S.-J., Zhang, M., and Dai, Y.: Description of the NCAR Community Atmosphere Model (CAM 3.0). Technical Report NCAR/TN-464+STR, National Center for Atmospheric Research, Boulder, CO, 226 pp., 2004.
- Dee, D. P., Uppala, S. M., Simmons, A. J., Berrisford, P., Poli, P., Kobayashi, S., Andrae, U., Balmaseda, M. A., Balsamo, G., Bauer, P., Bechtold, P., Beljaars, A. C. M., van de Berg, L., Bidlot, J., Bormann, N., Delsol, C., Dragani, R., Fuentes, M., Geer, A. J., Haimberger, L., Healy, S. B., Hersbach, H., Hólm, E. V., Isaksen, I., Kållberg, P., Köhler, M., Matricardi, M., McNally, A. P., Monge-Sanz, B. M., Morcrette, J.-J., Park, B.-K., Peubey, C., de Rosnay, P., Tavolato, C., Thépaut, J.-N., and Vitart, F.: The ERA-Interim reanalysis: Configuration and performance of the data assimilation system, *Q. J. Roy. Meteorol. Soc.*, 137, 553–597, 2011.
- Fletcher, C. G. and Kushner, P. J.: The role of linear interference in the Annular Mode response to Tropical SST forcing, *J. Climate*, 24, 778–794, doi:10.1175/2010JCLI3735.1, 2011.
- Fletcher, C. G., Hardiman, S. C., Kushner, P. J., and Cohen, J.: The dynamical response to snow cover perturbations in a large ensemble of atmospheric GCM integrations, *J. Climate*, 22, 1208–1222, 2009.
- Frierson, D. M. W., Lu, J., and Chen, G.: Width of the Hadley cell in simple and comprehensive general circulation models, *Geophys. Res. Lett.*, 34, L18804, doi:10.1029/2007GL031115, 2007.
- Fu, Q. and Lin, P.: Poleward shift of subtropical jets inferred from satellite-observed lower stratospheric temperatures, *J. Climate*, doi:10.1175/JCLI-D-11-00027.1, 2011.
- Fu, Q., Johanson, C. M., Wallace, J. M., and Reichler, T.: Enhanced mid-latitude tropospheric warming in satellite measurements, *Science*, 312, 1179, doi:10.1126/science.1125566, 2006.
- Gallego, D., Ribera, P., Garcia-Herrera, R., Hernandez, E., and Gimeno, L.: A new look for the Southern Hemisphere jet stream, *Climate Dyn.*, 24, 607–621, 2005.
- Haigh, J. D., Blackburn, M., and Day, R.: The response of tropospheric circulation to perturbations in lower-stratospheric temperature, *J. Climate*, 18, 3672–3685, 2005.
- Haynes, P. H., Marks, C. J., McIntyre, M. E., Shepherd, T. G., and Shine, K. P.: On the “downward control” of extratropical diabatic circulations by eddy-induced mean zonal forces, *J. Atmos. Sci.*, 48, 651–678, 1991.
- Held, I. M.: The general circulation of the atmosphere, paper presented at 2000 Woods Hole Oceanographic Institute Geophysical Fluid Dynamics Program, Woods Hole Oceanographic Institute, Woods Hole, Mass, available at: <http://www.whoi.edu/page.do?pid=13076>, 2000.
- Held, I. M. and Soden, B. J.: Robust responses of the hydrological cycle to global warming, *J. Climate*, 19, 5686–5699, 2006.
- Hu, Y. and Fu, Q.: Observed poleward expansion of the Hadley circulation since 1979, *Atmos. Chem. Phys.*, 7, 5229–5236, doi:10.5194/acp-7-5229-2007, 2007.
- Hudson, R. D., Andrade, M. F., Follette, M. B., and Frolov, A. D.: The total ozone field separated into meteorological regimes – Part II: Northern Hemisphere mid-latitude total ozone trends, *Atmos. Chem. Phys.*, 6, 5183–5191, doi:10.5194/acp-6-5183-2006, 2006.
- Johanson, C. M. and Fu, Q.: Hadley cell widening: Model simulations versus observations, *J. Climate*, 22, 2713–2725, 2009.
- Kalnay, E., Kanamitsu, M., Kistler, R., Collins, W., Deaven, D., Gandin, L., Iredell, M., Saha, S., White, G., Woollen, J., Zhu, Y., Leetmaa, A., Reynolds, B., Chelliah, M., Ebisuzaki, W., Higgins, W., Janowiak, J., Mo, K. C., Ropelewski, C., Wang, J., Jenne, R., and Joseph, D.: The NCEP/NCAR 40-year reanalysis project, *B. Am. Meteorol. Soc.*, 77, 437–471, 1996.
- Kanamitsu, M., Ebisuzaki, W., Woollen, J., Yang, S.-K., Hnilo, J. J., Fiorino, M., and Potter, G. L.: NCEP-DOE AMIP-II Reanalysis (R-2), *B. Am. Meteorol. Soc.*, 83, 1631–1643, 2002.
- Kidston, J. and Gerber, E. P.: Intermodel variability of the poleward shift of the austral jet stream in the CMIP3 integrations linked to biases in 20th century climatology, *Geophys. Res. Lett.*, 37, L09708, doi:10.1029/2010GL042873, 2010.
- Kidston, J., Dean, S. M., Renwick, J. A., and Vallis, G. K.: A robust increase in the eddy length scale in the simulation of future climates, *Geophys. Res. Lett.*, 37, L03806, doi:10.1029/2009GL041615, 2010.
- Kidston, J., Vallis, G. K., Dean, S. M., and Renwick, J. A.: Can the increase in the eddy length scale under global warming cause the poleward shift of the jet streams?, *J. Climate*, 24, 3764–3780, doi:10.1175/2010JCLI3738.1, 2011.
- Koch, D., Schulz, M., Kinne, S., McNaughton, C., Spackman, J. R., Balkanski, Y., Bauer, S., Bernsten, T., Bond, T. C., Boucher, O., Chin, M., Clarke, A., De Luca, N., Dentener, F., Diehl, T., Dubovik, O., Easter, R., Fahey, D. W., Feichter, J., Fillmore, D., Freitag, S., Ghan, S., Ginoux, P., Gong, S., Horowitz, L., Iversen, T., Kirkevåg, A., Klimont, Z., Kondo, Y., Krol, M., Liu, X., Miller, R., Montanaro, V., Moteki, N., Myhre, G., Penner, J. E., Perlwitz, J., Pitari, G., Reddy, S., Sahu, L., Sakamoto, H., Schuster, G., Schwarz, J. P., Seland, Ø., Stier, P., Takegawa, N., Takemura, T., Textor, C., van Aardenne, J. A., and Zhao, Y.: Evaluation of black carbon estimations in global aerosol models, *Atmos. Chem. Phys.*, 9, 9001–9026, doi:10.5194/acp-9-9001-2009, 2009.
- Kushner, P. J. and Polvani, L. M.: Stratosphere-troposphere coupling in a relatively simple AGCM: The role of eddies, *J. Climate*, 17, 629–639, 2004.
- Kushner, P. J., Held, I. M., and Delworth, T. L.: Southern Hemisphere atmospheric circulation response to global warming, *J. Climate*, 14, 2238–2249, 2001.
- Lindzen, R. S. and Farrell, B.: A simple approximate result for the maximum growth rate of baroclinic instabilities, *J. Atmos. Sci.*, 37, 1648–1654, 1980.
- Lorenz, D. J. and DeWeaver, E. T.: Tropopause height and zonal wind response to global warming in the IPCC scenario integrations, *J. Geophys. Res.*, 112, D10119, doi:10.1029/2006JD008087, 2007.
- Lu, J., Vecchi, G. A., and Reichler, T.: Expansion of the Hadley cell under global warming, *Geophys. Res. Lett.*, 34, L06805,

- doi:10.1029/2006GL028443, 2007.
- Lu, J., Chen, G., and Frierson, D. M. W.: Response of the zonal mean atmospheric circulation to El Niño versus global warming, *J. Climate*, 21, 5835–5851, 2008.
- Lu, J., Deser, C., and Reichler, T.: Cause of the widening of the tropical belt since 1958, *Geophys. Res. Lett.*, 36, L03803, doi:10.1029/2008GL036076, 2009.
- Newchurch, M. J., Yang, E.-S., Cunnold, D. M., Reinsel, G. C., Zawodny, J. M., and Russell III, J. M.: Evidence for slowdown in stratospheric ozone loss: First stage of ozone recovery, *J. Geophys. Res.*, 108, 4507, doi:10.1029/2003JD003471, 2003.
- Oleson, K. W., Dai, Y., Bonan, G., Bosilovich, M., Dickinson, R., Dirmeyer, P., Hoffman, F., Houser, P., Levis, S., Niu, G.-Y., Thornton, P., Vertenstein, M., Yang, Z.-L., and Zeng, X.: Technical description of the Community Land Model (CLM). Technical Report NCAR/TN-461+STR, National Center for Atmospheric Research, Boulder, CO, 174 pp., 2004.
- Polvani, L. M. and Kushner, P. J.: Tropospheric response to stratospheric perturbations in a relatively simple general circulation model, *Geophys. Res. Lett.*, 29, 1114, doi:10.1029/2001GL014284, 2002.
- Polvani, L. M., Waugh, D. W., Correa, G. J. P., and Son, S.-W.: Stratospheric ozone depletion: The main driver of twentieth-century atmospheric circulation changes in the Southern Hemisphere, *J. Climate*, 24, 795–812, 2011.
- Previdi, M. and Liepert, B. G.: Annular modes and Hadley cell expansion under global warming, *Geophys. Res. Lett.*, 34, L22701, doi:10.1029/2007GL031243, 2007.
- Ramanathan, V. and Carmichael, G.: Global and regional climate changes due to black carbon, *Nature Geosci.*, 1, 221–227, 2008.
- Reichler, T., Dameris, M., and Sausen, R.: Determining the tropopause height from gridded data, *Geophys. Res. Lett.*, 30, 2042, doi:10.1029/2003GL018240, 2003.
- Rienecker, M. M., Suarez, M. J., Gelaro, R., Todling, R., Bacmeister, J., Liu, E., Bosilovich, M. G., Schubert, S. D., Takacs, L., Kim, G.-K., Bloom, S., Chen, J., Collins, D., Conaty, A., da Silva, A., Gu, W., Joiner, J., Koster, R. D., Lucchesi, R., Molod, A., Owens, T., Pawson, S., Pegion, P., Redder, C. R., Reichle, R., Robertson, F. R., Ruddick, A. G., Sienkiewicz, M., and Woollen, J.: MERRA: NASA's Modern-Era Retrospective Analysis for Research and Applications, *J. Climate*, 24, 3624–3648, 2011.
- Rind, D., Perlwitz, J., and Lonergan, P.: AO/NAO response to climate change: 1. Respective influences of stratospheric and tropospheric climate changes, *J. Geophys. Res.*, 110, D12107, doi:10.1029/2004JD005103, 2005.
- Scaife, A., Spanghel, T., Fereday, D., Cubasch, U., Lange-matz, U., Akiyoshi, H., Bekki, S., Braesicke, P., Butchart, N., Chipperfield, M., Gettelman, A., Hardiman, S., Michou, M., Rozanov, E., and Shepherd, T.: Climate change projections and stratosphere-troposphere interaction, *Climate Dyn.*, 38, 2089–2097, doi:10.1007/s00382-011-1080-7, 2012.
- Seidel, D. J. and Randel, W. J.: Recent widening of the tropical belt: Evidence from tropopause observations, *J. Geophys. Res.*, 112, D20113, doi:10.1029/2007JD008861, 2007.
- Seidel, D. J., Fu, Q., Randel, W. J., and Reichler, T. J.: Widening of the tropical belt in a changing climate, *Nature Geosci.*, 1, 21–24, doi:10.1038/ngeo.2007.38, 2008.
- Shindell, D. T., Schmidt, G. A., Miller, R. L., and Rind, D.: Northern Hemisphere winter climate response to greenhouse gas, ozone, solar, and volcanic forcing, *J. Geophys. Res.*, 106, 7193–7210, 2001.
- Shindell, D. T., Faluvegi, G., Lacis, A., Hansen, J., Ruedy, R., and Aguilar, E.: Role of tropospheric ozone increases in 20th-century climate change, *J. Geophys. Res.*, 111, D08302, doi:10.1029/2005JD006348, 2006.
- Smith, K. L., Fletcher, C. G., and Kushner, P. J.: The role of linear interference in the Annular Mode response to extratropical surface forcing, *J. Climate*, 23, 6036–6050, 2010.
- Smith, S. J., van Aardenne, J., Klimont, Z., Andres, R. J., Volke, A., and Delgado Arias, S.: Anthropogenic sulfur dioxide emissions: 1850–2005, *Atmos. Chem. Phys.*, 11, 1101–1116, doi:10.5194/acp-11-1101-2011, 2011.
- Thompson, D. W. J. and Wallace, J. M.: Annular modes in the extratropical circulation. Part I: Month to month variability, *J. Climate*, 13, 1000–1016, 2000.
- Uppala, S., Kallberg, P., Simmons, A., Andrae, U., Bechtold, V., Fiorino, M., Gibson, J., Haseler, J., Hernandez, A., Kelly, G., Li, X., Onogi, K., Saarinen, S., Sokka, N., Allan, R., Andersson, E., Arpe, K., Balmaseda, M., Beljaars, A., Van De Berg, L., Bidlot, J., Bormann, N., Caires, S., Chevallier, F., Dethof, A., Dragosavac, M., Fisher, M., Fuentes, M., Hagemann, S., Holm, E., Hoskins, B., Isaksen, I., Janssen, P., Jenne, R., McNally, A., Mahfouf, J., Morcrette, J., Rayner, N., Saunders, R., Simon, P., Sterl, A., Trenberth, K., Untch, A., Vasiljevic, D., Viterbo, P., and Woollen, J.: The ERA-40 re-analysis, *Q. J. R. Meteorol. Soc.*, 131, 2961–3012, 2005.
- van Aardenne, J. A., Dentener, F. J., Olivier, J. G. J., Goldewijk, C. G. M. K., and Lelieveld, J.: A 1 x 1 degree resolution dataset of historical anthropogenic trace gas emissions for the period 1890–1990, *Global Biogeochem. Cy.*, 15, 909–928, 2001.
- Wang, S., Gerber, E. P., and Polvani, L. M.: Abrupt circulation responses to tropical upper tropospheric warming in a relatively simple stratosphere-resolving AGCM, *J. Climate*, in press, 2012.
- Wilks, D. S.: *Statistical Methods in the Atmospheric Sciences*, Academic Press, 467 pp., 1995.
- Williams, G. P.: Circulation sensitivity to tropopause height, *J. Atmos. Sci.*, 63, 1954–1961, 2006.
- Yin, J. H.: A consistent poleward shift of the storm tracks in simulations of 21st century climate, *Geophys. Res. Lett.*, 32, L18701, doi:10.1029/2005GL023684, 2005.
- Zhou, Y. P., Xu, K.-M., Sud, Y. C., and Betts, A. K.: Recent trends of the tropical hydrological cycle inferred from Global Precipitation Climatology Project and International Satellite Cloud Climatology Project data, *J. Geophys. Res.*, 116, D09101, doi:10.1029/2010JD015197, 2011.